Climate-induced storminess forces major increases in future storm surge hazard in the South China Sea region

Melissa Wood[1], Ivan D. Haigh[1], Le Quan Quan[2], Nguyen Nghia Hung[2], Tran Ba Hoang[2], Stephen E. Darby[3], Robert Marsh[2], Nikolaos Skliris[2], Joël J.-M. Hirschi[4], Robert J. Nicholls[5], and Nadia Bloemendaal[6]

[1] School of Ocean and Earth Science, National Oceanography Centre Southampton, University of Southampton, Waterfront Campus, European Way, Southampton, UK
[2] Southern Institute of Water Resource Research (SIWRR), 658th Vo Van Kiet Avenue, Ward 1, District 5, Ho Chi Minh city, Vietnam
[3] School of Geography and Environmental Science, University of Southampton, Highfield, Southampton, UK
[4] National Oceanography Centre Southampton, University of Southampton, UK
[5] Tyndall Centre for Climate Change Research, University of East Anglia, Norwich, UK
[6] Institute for Environmental Studies (IVM), Vrije Universiteit Amsterdam, 1081 HV, Amsterdam, The Netherlands

Correspondence to: Ivan Haigh (I.D.Haigh @soton.ac.uk)

Abstract

It is vital to robustly estimate the risks posed by extreme sea levels, especially in tropical regions where cyclones can generate large storm surges and observations are too limited in time and space to deliver reliable analyses. To address this limitation for the South China Sea region, we force a hydrodynamic model with a new synthetic database representing 10,000 years of past/present and future tropical cyclone activity, to investigate climate change impacts on extreme sea levels forced by storm surges (with and without tides). We show that, as stronger and more numerous tropical cyclones likely pass through this region over the next 30 years the severity of storm surge hazard increases, particularly around Vietnam and China coastlines. The spatial extent of tropical cyclone activity is greater and extreme storm surge events in this region become a more frequent occurrence in the future too. This threatens low-lying, densely-populated areas such as the major river deltas in this region, while sections of the Cambodian and Thai coastline face previously unseen storm surge hazards. These future hazards strongly signal that coastal flood management and adaptation in these areas should be reviewed for their resilience against future extreme sea levels.

1 Introduction

It is estimated that currently almost 230 million people around the world are directly exposed to some level of storm surge hazard from either tropical or extra-tropical cyclone activity, based on SwissRe global models (SwissRe, 2017). The populations most acutely at risk from storm surge induced extreme sea levels are those located on low-lying coastlines within tropical zones associated with intense cyclone activity (Dullaart et al., 2021; Edmonds et al., 2020; Kirezci et al., 2020; Woodruff et al., 2013; McGranahan et al., 2007; see also supplementary material section 1). Given this vulnerability, the knowledge around how much sea level extremes are influenced by tides, storm surges and waves is not well developed (Fox-Kemper et al., 2021). In fact, global assessments regularly overlook the contribution of low probability Tropical Cyclone (TC) events towards storm surge induced extreme sea level flooding (Dullaart et al. 2021; Muis et al., 2016).

This knowledge shortfall is in large part because of the essential difficulty of assessing tropical-cyclone induced storm surge datasets associated with events that are, by their very nature, somewhat infrequent (Dullaart et al., 2021; Mori et al., 2019). TCs are not only rare events, but they typically affect comparatively short stretches of coastline (<500km) as they approach land, and so storm surges are under-represented in the data from the sparsely distributed network of global tide gauges (Bloemendaal et al., 2020; Pugh and Woodworth 2014). Furthermore, analysing extreme storm surge behaviour, and estimating storm surge hazard, ideally requires long (50-100 years) time series of sea level data, which do not exist in most tropical regions (Irish et al., 2011). This limitation is acutely problematic because extreme sea level statistics, that define storm surge hazard, based on short records are notoriously imprecise (Kirezci et al., 2020; Lin and Emanuel 2016; Irish et al., 2011).

To overcome these problems, previous studies have adopted two different approaches with the same goal of extending the historic sea level record available from existing tide gauge data. The first approach is to reconstruct multi-decadal storm surge signals through the use of statistical models to infer surge time-series from more widely available meteorological datasets. These methods use simple linear or multiple regression models on climate

indices to reconstruct long time series of surge levels from which extreme values and trends can be more robustly estimated. This has been done at both regional and global scales, using, for example, the tide gauge record and 20th Century Reanalysis data (Zhang and Wang 2021; Cid et al., 2017, 2018) or a mixture of climate reanalyses data (Wahl and Chambers 2016; Tadesse and Wahl 2021). Statistical approaches mostly benefit from modest computational resource needs, but this advantage is traded-off against the use of meteorological forcings that often have insufficient spatial resolution in tropical regions to capture the effects of cyclone activity on sea levels (Cid et al., 2018; Haigh et al., 2014).

The second approach involves the use of hydrodynamic models to generate multi-decadal time-series of surge-driven extreme sea levels across oceanic domains. TC induced storm surges are challenging to model at continental or global scales because these storms typically have sizes less than the model mesh resolution, or are smoothed out in the large grid cells of meteorological datasets, and are therefore difficult to resolve (Kirezci et al., 2020; Bloemendaal et al., 2019b; Takagi et al., 2017; Larson et al., 2014; Murakami and Sugi 2010). An earlier version of the Global Tide and Surge Model (GTSM, Muis et al. 2016) using ERA-Interim data was found to underestimate TC induced extreme sea levels for this reason. This problem was subsequently overcome in the latest (GTSMv3) iteration, with an updated model resolution and use of ERA5 reanalysis climate data, to successfully simulate past and present extreme sea levels (Muis et al. 2020; C3S 2017).

To address the scarcity of adequate storm surge components within extreme sea level analysis, several studies have recently attempted to force numerical storm surge models with synthetic datasets that seek to represent long-term TC activity. For example, Haigh et al. (2014) extended the work of Harper et al., (2009) and generated a 10,000 year synthetic dataset of TC activity for the Australian region. These atmospheric data were used to force a MIKE 21 hydrodynamic of the Australian coastline and produce a 61-year hindcast of sea levels from which to estimate present day exceedance probabilities due to storm surge. More recently Bloemendaal et al., (2020) similarly developed a Synthetic TC geneRation Model (STORM) dataset which statistically resampled and simulated TC tracks and intensities from 38 years of historical atmospheric data from the International Best Track Archive for Climate Stewardship dataset (IBTrACS; Knapp et al., 2010) to the equivalent of 10,000 years under the same climate conditions. Dullaart et al., (2021) subsequently coupled this STORM data with the GTSMv3 model to produce past/present (1980-2018) storm tides and sea level return period estimates for coastlines world-wide, directly confronting the problems of precision in relative location (of tide gauges) and availability of storm data.

Looking to the future, coastal flood hazard is expected to increase, primarily due to rising mean sea level, but also due to possible change in tides, storm surges, and wave set-up (Kirezci et al., 2020; Haigh et al., 2020). Kirezci et al. (2020) calculated that, by 2100, between 2.5% and 4.1% of the world's population is estimated to be at risk of extreme (specifically 1:100 year Annual Exceedance Probability or 1% AEP) coastal flooding from this combination of hazards, under the mean SSP5-8.5 scenarios and assuming no flood protection. In contrast to the large number of studies that have focused on changes in global mean sea-levels, much less research has been devoted to determining the contribution of climate-driven changes in storm activity in forcing extreme sea levels. While there is consensus that there will be substantial changes to the frequency and severity of tropical (and extra-tropical/mid-latitude) cyclones in the future, the two most recent reports of the Intergovernmental Panel on Climate Change (IPCC) underscore that there is currently '*low confidence*' (~ 20% chance) in our ability to

correctly predict how climate-driven storm surges may contribute to changes in future sea level extremes (Emanuel 2021; Fox-Kemper et al., 2021; Knutson et al., 2020; Wahl et al., 2017; Wong et al., 2014; Woodruff et al., 2013; Mousavi et al., 2011). This deep uncertainty arises not only from the significant challenge of predicting changes in tropical (and mid-latitude) cyclone activity at a regional scale, but also because of the small number of storm surge studies available at the time of the last IPCC Assessment Review.

Most past studies have assumed to date that storm surge extreme behaviour has been, and will continue to be, stationary and that the extreme wave climate will change little over large ocean regions (Vitousek et al, 2017; Hinkel et al., 2014). But with projections of a changed climate by the end of this century, this hypothesis has been challenged in recent global and local modelling studies (e.g. Tadesse and Wahl, 2021; Lin-Ye et al., 2020). For European coastlines by 2100, modelling shows that extreme storm surge levels may augment relative sea-level rise by over 30%, under the mean SSP5-8.5 climate projections (Vousdoukas et al., 2016). More recently Calafat et al. (2022) examined 1960-2018 tide gauge observations for north-western European seas and discovered changed trends in surge extremes due to climate variability and anthropogenic forcing. This trend has already affected the likelihood of surge extremes in this region. This therefore puts into question how effective current coastal flood defences actually are now against present storm surge hazard (having been originally designed under the assumption of stationary surge extremes), but it also has strong implications for future coastal planning in this region.

The Western North Pacific (WNP) basin region currently accounts for almost one-third of all TC counts globally (Gray 1977, 1975). Moreover, 8 of the 10 most densely populated areas at risk from storm surges are located in Asia (SwissRe, 2017). South-east Asia has long been identified as a 'hotspot' for projected future mean sea-level rise, plus extremes of sea level related to storm activity (Nicholls et al., 2021; Kirezci et al., 2020; Nicholls and Cazenave, 2010; McGranahan et al., 2007). WNP TCs (typhoons) are projected to become more intense over the course of the 21st century, with higher category cyclones increasing in frequency (Emanuel 2021; Knutson et al., 2020; Lap, 2019; Emanuel 2013; Woodruff et al., 2013; Zang and Church 2012; Chan, 2005). Consequently, in this paper we aim to better understand storm surge and extreme sea level behaviour in a tropical zone of intense TC activity, now and into the future, by creating a hydrodynamic coastal model to simulate TC induced storm surge hazard for the South China Sea region. Given that our project partnerships provide particular expertise and data for Vietnam (Hung et al., 2012), a side-objective is to assemble a more detailed analysis for Vietnam coastlines for future study. The hydrodynamic model of the South China Sea incorporates wind and pressure data from two state-of-the-art synthetic STORM datasets for the WNP region representing present and future TC tracks. As already stated, STORM datasets contain a wealth of synthetic storm-years of TC data, and ensures that even very low probability, but highly hazardous extreme sea levels can, for the first time, be fully represented in a regional analysis.

The paper is structured as follows. A description of the hydrodynamic model and STORM data used is provided in Section 2, incorporating a description of the model configuration and validation (against tides and measured storm surge data) and the approach used to determine return period sea levels from our model outputs. Section 3 details the results obtained from simulating STORM synthetic TC data in the coastal model, including the range of return periods obtained for both storm surge-only and tide-surge scenarios. Sections 4 and 5 thereafter discuss the results and implications, and summarise our conclusions respectively.

2 Data and methods

The tools, data and methodology used in this study are described in this section. Section 2.1 relates to the hydrodynamic model, describing the set up (2.1.1) and the process and data used for validation of tides (2.1.2) and storm surge (2.1.3). Then section 2.2 is dedicated to the forcing data used to define TC activity in the model, first describing the STORM dataset (2.1.1), how it was incorporated into the model (2.1.2) and then finally a description of the methods we used to obtain storm surge return periods (2.1.3).

2.1 The hydrodynamic model

We introduce here the hydrodynamic model, first outlining the model configuration and the specification of local tides. We then document validation of simulated tides and storm surges in the model, using available tide gauge data.

2.1.1 Model configuration

We updated a DHI MIKE 21 FM (DHI, 2017a) depth-averaged barotropic, hydrodynamic model of the South China Sea; provided by our Vietnam partners on the project (the Southern Institute of Water Resource Research, SIWRR), to simulate local sea levels (Fig. 1a). The MIKE 21 FM (flexible mesh) model uses an irregular triangular mesh to represent the domain area. This type of mesh provides computation efficiencies by optimising element size to range between coarse resolution for deep ocean to a more precise representation around detailed coastlines or for features of particular interest.

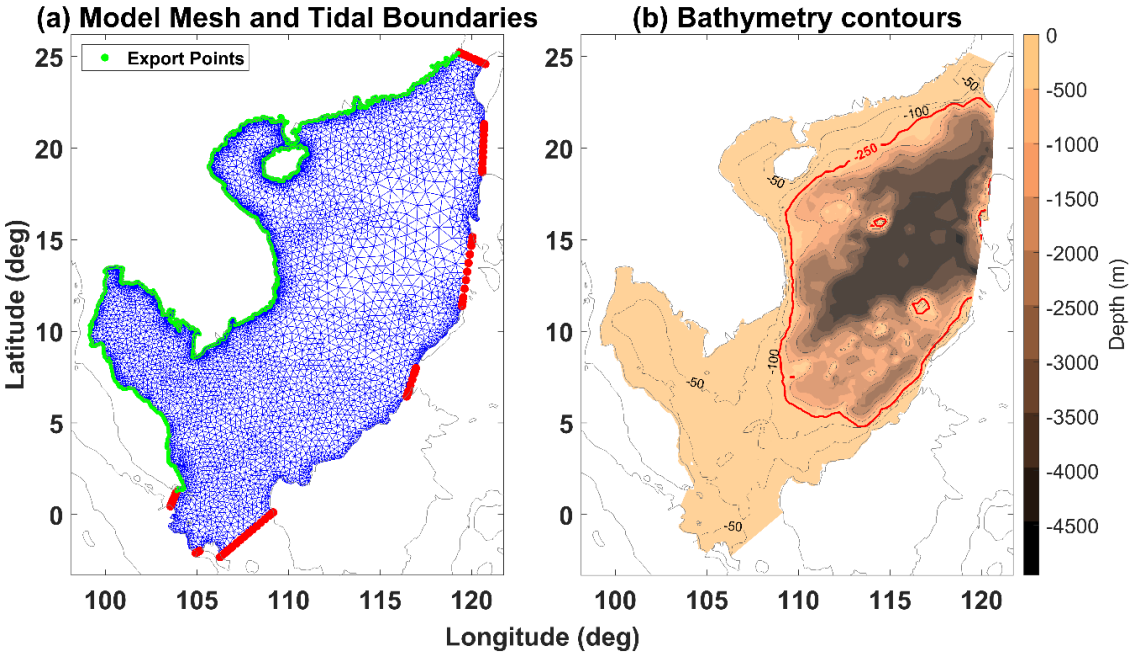

Figure 1 – (a) MIKE 21 FM bathymetry and model mesh for the South China Sea. The irregular triangular mesh grid (blue) of the model has tidal boundaries shown in red. The OCP coastline points exported from the model for analysis are also shown (green). (b): SRTM15+ ocean bathymetry for our South China Sea domain, showing nearshore -50m and -100m contours as well as the -250m depth contour (red) approximating the edge of the continental shelf.

We updated the original model land boundary with the Prototype Global Shoreline data from the National Geospatial Intelligence Agency (via National Oceanic and Atmospheric Administration; https://shoreline.noaa.gov). To create a model which could be run around one hundred thousand times, but still offer fair accuracy, we selected grid resolutions at the model's coastal boundaries of ~11 km , reducing to ~7 km and ~5.5 km for the shorelines of Cambodia, Thailand and China around Hainan island immediately adjacent to Vietnam. This resolution becomes finer again at ~2.3 km along the coastline of Vietnam itself. For mesh representing deep water, the grid is not more than ~83 km across. The mesh size at each the seven open sea boundaries, is approximately ~52 km in the model.

For bathymetry, we replaced the data in the original model with a 15 arcseconds resolution global dataset from SRTM15+ (v2). This bathymetry data (Fig. 1b) was downloaded from the Scripps Institution of Oceanography website (https://topex.ucsd.edu; Tozer, et al., 2019) and interpolated onto the model grid. All model data therefore is measured using an EGM96 vertical reference datum.

Because the model is barotropic, ocean currents are not separately incorporated. No wave modelling was carried out in this analysis either, since the focus of this paper is to be on still sea level. Tides were only separately modelled for validation and to estimate total water levels. To simulate tides we generated the astronomical tidal component within the domain using tide data obtained from the Oregon State University Tidal Inversion Software (OTIS, Martin et al., 2009; Egbert & Erofeeva 2002). The harmonic constituents were downloaded from the OTIS web site (http://volkov.oce.orst.edu/tides/) for the seven model open sea boundaries of our model. The data are provided for eight primary (M2, S2, N2, K2, K1, O1, P1, Q1), two long period (Mf, Mm) and three non-linear (M4, MS4, MN4) harmonic constituents. With these data, the tide was then predicted, for each boundary grid point, using the Tidal Model Driver (TMD) MATLAB toolbox (http://polaris.esr. org/ptm_index.html) with the 'China Seas and Indochina region (2016)' tidal model option. These open sea boundaries were only used to force conditions in tide-only model simulations for tide validation (2.1.2), and then later to aid the calculation of total water levels (2.2.3 & 3.2).

2.1.2 Model validation: tides

We undertake two validation exercises to ensure that our MIKE 21 FM model accurately captures the complex tidal characteristics of the modelled region (Phan et al., 2019). The first tide validation was to simply compare model-simulated and observed tide levels directly and quantify the error. Observed hourly sea level data was obtained at 27 tide gauge stations located around the South China Sea (Fig. 2; Caldwell, et al., 2015). Extra years of sea level data at four of these tidal gauges (Phu Quoc, Phu Quy, Son Tra, Rach Gia) was also made available directly from our project partners at SIWRR. Despite there being a good number of tide gauges in the South China Sea region, only a third (Kaohsiung, Hong Kong, Ko Lak, Geting, Cendering, Kuantan, Sedili and Vung Tau) have 30 or more years of data. Therefore, to overcome the problem of an incomplete data record at some tide gauge locations, and to remove the major meteorological influences, we carried out a two-step pre-processing of the observed data record. The first step was to undertake a harmonic analysis on the available observed levels using the MATLAB T-Tide software (Pawlowicz et al. 2002) to extract the tidal components. We obtained the standard set of 67 tidal constituents, for the most recent year (2019) with the least amount of missing data. We then used MATLAB T-Tide software again to apply the harmonic constituents and create an uninterrupted series of tide levels, for each gauged location in Table 1, for a randomly chosen month (January) in the year 2019. The

second step was to obtain annual mean sea level values for each tide gauge, and then subtract this level from the data, to offset each time-series so it was equivalent to the model datum of mean sea level.

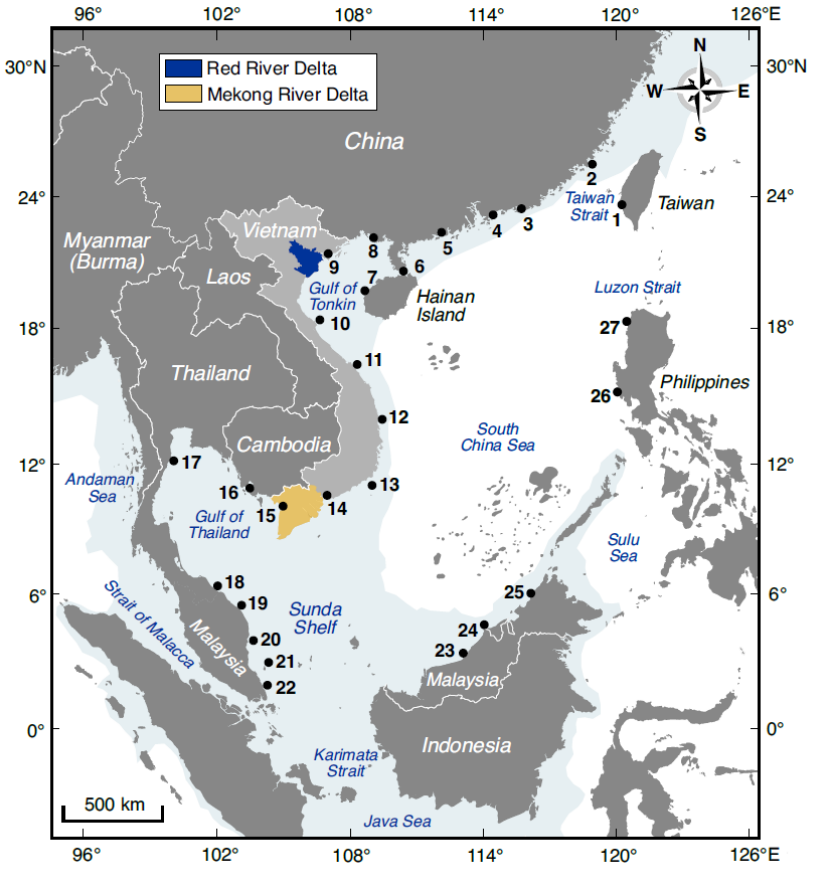

Figure 2 – South China Sea model domain, with location of tidal gauges numbered (also see Table 1) and the rough location of the Red and Mekong River Deltas highlighted. The shaded blue area, in-sea, shows the approximate coverage of the continental shelf, at ~250 m depth.

Table 1 - Validation of sea levels output by the model. Mean absolute difference errors (Mean Absolute Error - MAE) between modelled and observed tide gauge data, for January 2019, at each gauged location in Figure 2. The standard deviation around this MAE is also given.

Tide Gauge	***ID (Fig. 2)***	***Latitude (degrees)***	***Longitude (degrees)***	**date range and [number of years of data available]**	**Mean absolute error (MAE, m)**	**Standard deviation of MAE (m)**	**Correlation Coefficient**
Kaohsiung	*1*	*22.61*	*120.28*	1980-2016 [37]	0.07	0.05	0.95
Xiamen	*2*	*24.42*	*118.30*	1954-1997 [28]	0.29	0.20	0.97
Shanwei	*3*	*22.65*	*115.30*	1975-1997 [23]	0.10	0.08	0.95
Hong Kong	*4*	*22.27*	*114.38*	1962-2018 [33]	0.13	0.11	0.93
Zhapo	*5*	*21.50*	*111.78*	1975-1997 [23]	0.12	0.09	0.97
Haikou	*6*	*20.02*	*110.28*	1976-1997 [22]	0.24	0.17	0.77
Dongfang	*7*	*19.10*	*108.62*	1975-1997 [23]	0.16	0.12	0.94
Beihai	*8*	*21.48*	*108.98*	1975-1997 [23]	0.20	0.13	0.98

Tide Gauge	***ID (Fig. 2)***	***Latitude (degrees)***	***Longitude (degrees)***	**date range and [number of years of data available]**	**Mean absolute error (MAE, m)**	**Standard deviation of MAE (m)**	**Correlation Coefficient**
Hon Dau	*9*	*20.67*	*106.82*	1995 [1]	0.32	0.25	0.89
Vung Ang	*10*	*18.18*	*106.35*	1996-1997 [2]	0.21	0.14	0.81
Son Tra	*11*	*16.10*	*108.22*	2009 [1]	0.09	0.07	0.96
Qui Nhon	*12*	*13.77*	*109.38*	1994-2018 [22]	0.16	0.13	0.85
Phu Quy	*13*	*10.52*	*108.93*	2008-2009 [2]	0.20	0.14	0.87
Vung Tau	*14*	*10.34*	*107.01*	1980-2018 [39]	0.18	0.12	0.97
Rach Gia	*15*	*9.99*	*105.07*	1996-2018 [23]	0.12	0.09	0.84
Phu Quoc	*16*	*10.22*	*103.97*	2008-2009 [2]	0.08	0.06	0.91
Ko Lak	*17*	*11.79*	*99.90*	1985-2018 [34]	0.15	0.09	0.93
Geting	*18*	*6.25*	*102.12*	1986-2015 [30]	0.13	0.08	0.86
Cendering	*19*	*5.26*	*103.23*	1984-2015 [32]	0.16	0.11	0.92
Kuantan	*20*	*3.97*	*103.44*	1983-2015 [33]	0.19	0.12	0.93
Tioman	*21*	*2.81*	*103.60*	1985-2015 [31]	0.18	0.13	0.93
Sedili	*22*	*1.93*	*104.18*	1986-2015 [30]	0.19	0.13	0.90
Bintulu	*23*	*3.45*	*113.03*	1992-2015 [24]	0.13	0.09	0.95
Miri	*24*	*4.39*	*113.90*	1992-2014 [23]	0.08	0.06	0.97
Kota Kinabalu	*25*	*5.98*	*116.07*	1987-2015 [29]	0.14	0.11	0.93
Subic Bay	*26*	*9.75*	*118.30*	2007-2018 [12]	0.07	0.06	0.96
Currimao	*27*	*14.76*	*120.00*	2009-2018 [10]	0.05	0.04	0.97

To create a matching record of model-simulated tide levels, the hydrodynamic model was run in tide-only mode – i.e. simply with OTIS-derived open sea boundary levels and no meteorological forcing - for the same month of January 2019. Hourly results were output for the grid points located closest to the 27 tide gauge coordinates. The resulting time-series of model-simulated and observed tide levels is shown in Fig. 3, for six gauge locations at the Vietnamese coastline. With this data, we calculated the Mean Absolute Error (MAE), and the standard deviation around this MAE, for all 27 grid points (Table 1). The average of all these MAE is 0.15 m, and the average of all the grid points' standard deviation is 0.1 m. This size difference error is consistent with earlier studies simulating extreme sea levels (e.g., Muis et al., 2016; Vousdoukas et al., 2016; Haigh et al., 2014). Table 1 also reveals that locations where tide gauges record diurnal tides, around the Gulf of Tonkin (6-9 in Fig. 2), had the largest MAE and standard deviation of absolute difference error, whereas the locations where tide gauges record semi-diurnal and mixed tides around Vietnam, Borneo and China coastlines (stations 1-5, 10-16, 18-26 in Fig. 2) had chiefly the smallest. The correlation coefficients in Table 1 ranged between 0.77 and 0.98 with the highest correlations in the northern and eastern areas of the model that experience fully- or mainly- semi-diurnal tidal regimes.

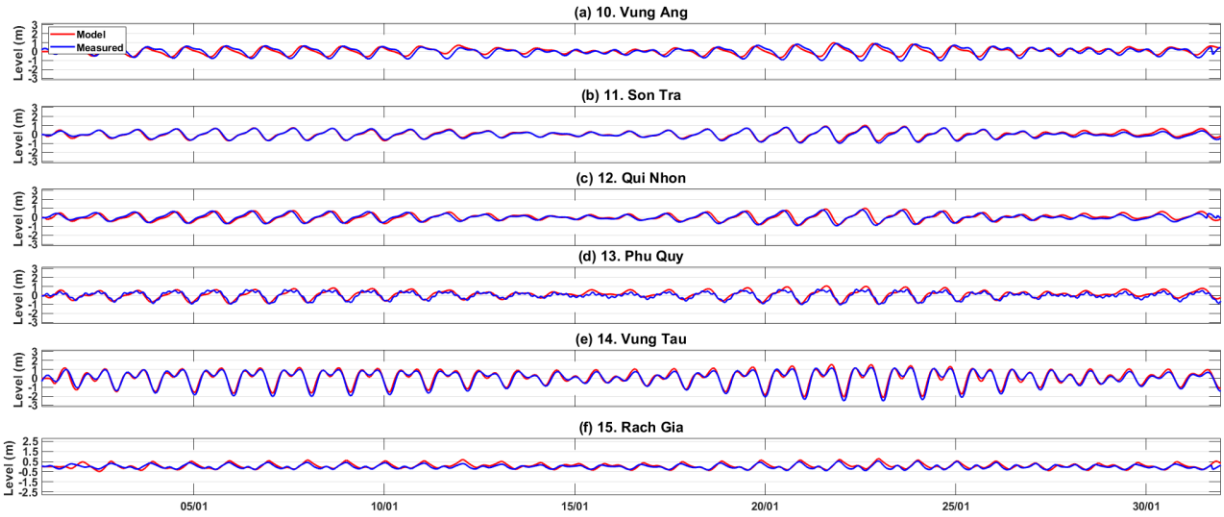

Figure 3 - Comparison of modelled (red) and measured (blue) sea level time series (January 2019) at six Vietnamese tide gauge station locations (see Figure 2 for locations)

The second tide validation exercise examines the amplitude and phase difference of the four main tidal constituents, extracted from the model-simulation and observed time-series at each of the 27 sites. The mean absolute amplitude and phase errors of the four main tidal constituents (M_2, S_2, O_1 and K_1), across all 27 tide gauge sites, is shown in Table 2. The model accurately matches tidal constituent observations for most stations. The MAE on tidal amplitude of the four main tidal constituents, are 0.05, 0,03, 0.06 and 0.06 m, respectively. There is a slight amplitude underestimation where there are transitioning tidal regimes; such as the amplitude of larger semi-diurnal tides around the Taiwan strait (Xiamen) and mixed diurnal tides around the Gulf of Tonkin. The mean absolute phase error of the M_2, S_2, O_1 and K_2 constituents are 17, 18, 11 and 12 degrees, respectively (Table 2). Small semi-diurnal (M_2 and S_2) phase differences exist in the model for stations located around the mixed (mainly diurnal) tide zones of central Vietnam. Phase and amplitude errors may be due to the absolute decimal accuracy of some tide gauge location coordinates as much as due to model limitations. This comparison between model-simulated and observed tide levels shows that the model does accurately replicate the tidal signals and captures both tidal range and form variations for the entire region.

Table 2 - Mean absolute amplitude and phase errors of the four main tidal constituents for the 27 validation sites.

Tidal Constituent	**Mean absolute amplitude error (cm) [s.d.]**	**Median absolute phase error (degrees) [s.d.]**
M_2	5 [4]	16.8 [15]
S_2	3 [2]	18.4 [17]
O_1	6 [6]	11.3 [7]
K_1	6 [6]	11.8 [9]

2.1.3 Model validation: storm surges

The next validation exercise concerns examining the hydrodynamic model's ability to accurately simulate storm surges induced by TCs. The length of measured sea level data was, on average, short across all 27 gauge locations.

Consequently, only a small selection of large storm surges is represented in the available tide gauge records and we therefore focused on those select past cyclone events for validation.

The first step was to identify potential TCs in the South China Sea that we could model, using data from the IBTrACS version 4 database (https://www.ncdc.noaa.gov/ibtracs/; Knapp et al., 2010). We collated all cyclone events in IBTrACS for the WNP region and for the period 1970 to 2020, which: (1) made land fall; (2) have matching measured sea level data at a tide gauge close to the land fall location; and (3) capture the storm surge in the measured records for that event. Furthermore, radius to maximum winds information was only available in the IBTrACS data for certain cyclones and this therefore further reduced the possible number of cyclones for validation. A total of four cyclone events matched the above criteria: Typhoon Sally in September 1996; Tropical Storm Linda in October/November 1997; Typhoon Ketsana in September 2009; and Typhoon Mangkhut in September 2018. These cyclones impacted different stretches of coastline and thus provided a range of events suitable to validate the model.

The second step was to create spatially and temporally changing wind and pressure fields from ERA5 reanalysis (Hersbach et al., 2018) atmospheric data. These data were obtained from the Copernicus climate data store (https://cds.climate.copernicus.eu/), for the known cyclone dates, on a regular 0.25 degree x 0.25 degree grid at hourly resolution. Wind and pressure data were clipped to the area of interest and reformatted into a MIKE 21 FM grid file format without further modification. Four model simulations were then carried out to simulate TC-generated storm surges using ERA5 meteorological forcing data.

Thirdly we generate alternative spatially and temporally varying wind and atmospheric pressure fields from the TC observation IBTrACS database. This was achieved for each storm event, using a Holland cyclone model (Holland, 1980) approach. The IBTrACS cyclone 3-hourly timesteps, wind speeds, radius to maximum winds and track coordinates were each imported into the MIKE 21 Cyclone Wind Generation tool (DHI, 2017b) using the 'Single Vortex Holland' tool option, with the Holland B parameter estimated using the Holland Formula specified in Harper and Holland (1999). We generated unique cyclone wind and pressure files at 0.25 degree x 0.25 degree grid resolution to match ERA5 spatial resolution for fair comparison. The model was then run, for each TC event, to simulate response using IBTrACS meteorological forcing data.

The fourth and final step was to create a corresponding 'tides-only' run, without any meteorological forcing, so we could isolate the storm surge components in each simulation, for each of the identified four TC events.

Using these meteorological forcing methods, the hydrodynamic model was able to closely predict the total water level (i.e., tide plus storm surge component), at the nearest tide gauge to where the cyclone made landfall, for four historic TC events. Figure 4 contrasts the IBTrACS/Holland model-derived and ERA5 validation results for Typhoon Ketsana, which made landfall close to the tide gauge at Son Tra, Vietnam (station 11 in Fig. 2) in September 2009, producing a storm surge of approximately 1.5 m. A comparison of the modelled and measured total water levels for this event is shown in Fig. 4a, with the isolated storm surge component shown in Fig. 4b. While the simulations using the IBTrACS/Holland model approach does capture the height of both the maximum sea level and the storm surge component (MAE = 0.18 m), the simulation driven with the ERA5 meteorological forcing significantly underestimates both the maximum sea level and the storm surge component (MAE = 0.40 m). Similar results (shown in the supplementary material section 2), favouring the IBTrACS/Holland over ERA5 forcing approach, were obtained for the other three cyclone events considered also. Overall, these validation

findings provide confidence that the hydrodynamic model is able to accurately capture both total water levels and the storm surge component of cyclone events, when the Holland meteorological forcing approach is used to generate wind and pressure fields for the hydrodynamic model.

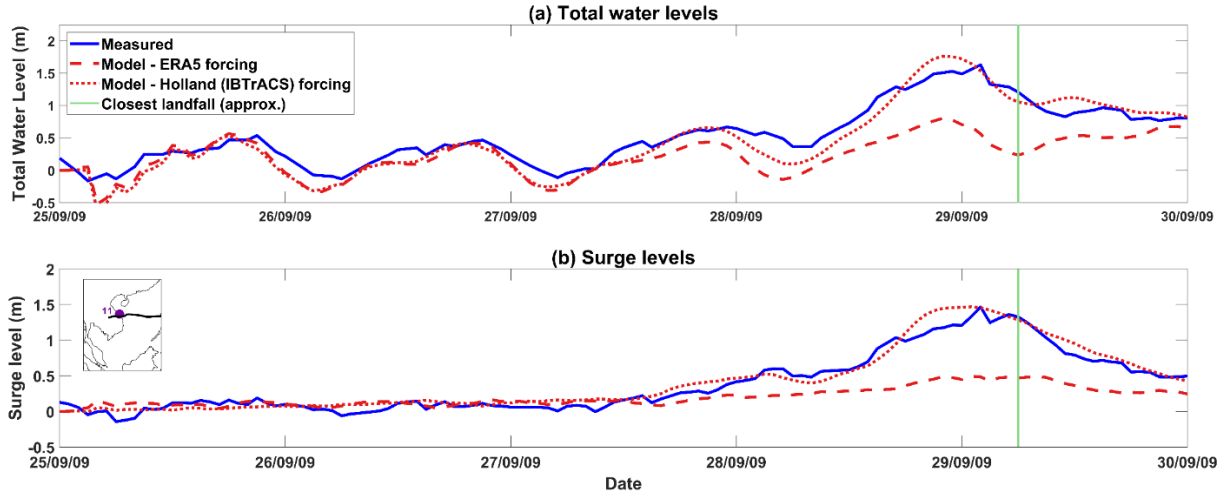

Figure 4 - Validating modelled surges using ERA5 (red dashed) and Holland Model using IBTrACS (red dotted) wind and pressure fields against measured data (blue): Typhoon Ketsana surge at tide gauge 11: Son Tra (inset or see Figure 2 for location). Firstly (a) comparing total water levels, and then (b) comparing surge-only sea levels. Typhoon Ketsana made landfall approximately 6am UTC on 29th September 2009 (green vertical line).

2.2 Simulating present and future extreme sea levels

We now present the methodology to show how extreme sea levels were generated within the hydrodynamic model – from simulating storm surges only, to estimating extreme sea levels (storm surge and tides together) and then to calculate the associated statistics. First, however, we outline the datasets used to obtain the necessarily large number of simulated TC events used in the model - for present day and for a future climate.

2.2.1 Two STORM datasets

To estimate extreme sea level in our model, we utilised synthetic TC data from the STORM (Statistically generated Tropical stORM) database. Bloemendaal et al. (2020) applied the STORM algorithm to TCs from 38 years of historical IBTrACS data (1980–2018) to statistically extend the original record into the equivalent of 10,000 years of TC activity and create the original past/present STORM database. The author's established that STORM preserves the TC statistics found within the original 38-year dataset. The database was developed to mimic the seasonality of the observed data it uses, so for TCs in south-eastern Asia, genesis occurs between May and November. The STORM database therefore provides 3-hourly, seasonally appropriate information on an individual cyclone's location, wind speed, pressure, radius to maximum winds and storm category. Further details, including a link to download the data itself, is available in the Bloemendaal et al. (2020) paper.

To create a sub-set of data for the period 1980-2018 for our own past/present hydrodynamic model we extracted all WNP area TCs that reach at least hurricane strength (Category 1 or greater on the Saffir-Simpson Hurricane Wind Scale; Simpson and Saffir, 1974) from the global STORM dataset (Bloemendaal et al. 2020). In the WNP,

this amounts to 156,879 cyclones. Then the database was further reduced by excluding TCs outside the model domain or those that were short lived (< 9 hours), leaving a sub-set of just over 30,800 individual cyclone-candidates for model simulation. This cropped down past/present dataset henceforth will be referred to as the baseline data sub-set.

Bloemendaal et al., (2022) later also created four new STORM future TC databases by similarly applying the STORM algorithm to extracted data from four climate models; CMCC-CM2-VHR4, CNRM-CM6-1, EC-Earth3P-HR and HadGEM3-GC31-HM. Each climate model was originally run at a high spatial resolution for the period 2015-2050 and forced with emissions representative of the SSP5-8.5 climate change scenario. The SSP5-8.5 climate change scenario represents unconstrained growth in economic output and energy, which exploits abundant fossil fuel resources and relies on global markets and technological progress to achieve sustainable development (IPCC, 2019). It is the highest greenhouse gas emissions pathway, linked to greater reliance on adaptation than mitigation to address climate challenges. Using a delta approach (contrasting present and future climate outcomes, see Bloemendaal et al., 2022), the authors then statistically created synthetic events representative of 10,000 years of TC activity, for each of the four future climate simulations. Overall, the STORM database has an observed trend for a greater proportion of cyclones to reach intense levels, compared to the baseline data (Bloemendaal et al., 2022 supplementary materials). Further details, including a link to download the original STORM data from a repository, can be found in the Bloemendaal et al. (2022) paper. We applied the above-described filtering method for all four future STORM datasets to determine TC frequency within our model domain (Table 3). This showed that while there would be a greater proportion of more intense (category 4-5 on the Saffir-Simpson scale) cyclones in the future South China Sea, the proportion of cyclones categorised as merely a tropical depression or tropical storm, would be considerably smaller also.

Table 3 – Number of baseline and future TCs of each category (using Saffir Simpson scale) within the reduced area of the model domain.

	Tropical Storm/Depression	**1**	**2**	**3**	**4**	**5**
STORM Present	54,255	29,114	14,410	13,003	5,938	120
STORM Future-CNRM	31,450	33,595	20,196	19,113	14,762	924
STORM Future-EC_Earth	34,018	35,000	19,736	18,254	12,375	657
STORM Future-HadGEM	30,409	33,322	20,923	20,202	13,213	491
STORM Future-CMCC	37,685	36,672	18,553	15,911	10,598	621

In order to avoid the large computational cost of simulating the storm surge conditions associated with the equivalent of 10,000 years of cyclone activity four times over, we elected to only use data from a single global climate model projection. The future STORM dataset based on the CNRM-CM6-1 climate model was selected as - in the range of available climate model options - it ranked in-between extremes for the number of more intense (category 4 and category 5) cyclones within the domain, and thus suggested a middle pathway from all the four climate models options (Table 3). We thus created our second sub-set of TC data from the 'CNRM-CM6-1 climate model' future STORM dataset (Bloemendaal et al. 2022) for our hydrodynamic model, by applying the same filtering procedure as for the baseline data above. After this we were left with over 63,300 individual cyclone tracks inside the model domain, of sufficient duration, covering the 2015-2050 period.

Figure 5 shows heatmaps of the resulting track density of TCs passing through the hydrodynamic model domain, for the: (a) baseline 1989-2018 period; and (b) future 2015-2050 period scenarios. Contrasting these two scenarios, each covering similar ~35 year timescales, shows that some locations are projected to experience greater number of TC tracks in the future, as highlighted in 'difference' plot of Fig. 5c. This projection suggest that the mid-Vietnam coastline is likely to experience an increase in TC strikes by the middle of the century.

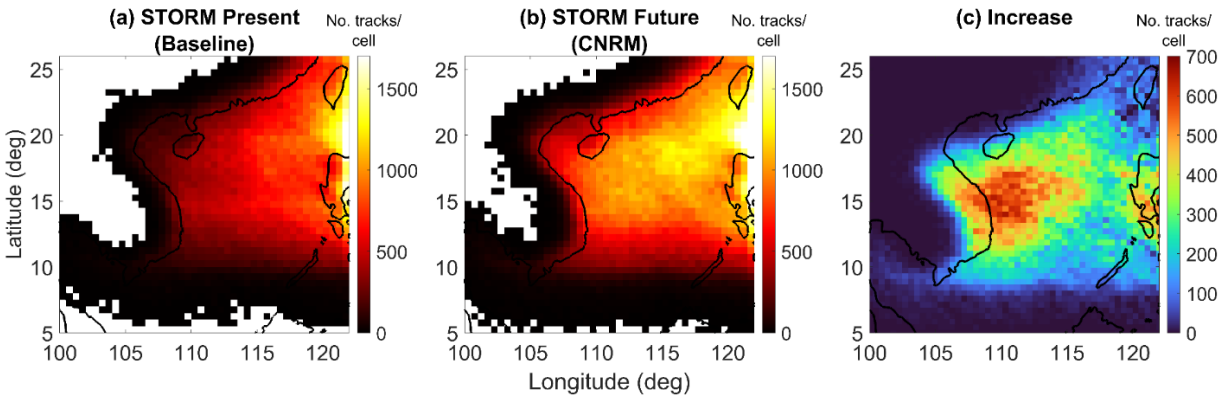

Figure 5 - Track density = the number of Saffir Simpson category 1-5 Tropical Cyclone tracks passing through each 0.5 degree x 0.5 degree grid cell within each ~35 year period. Left: Baseline STORM track density of Saffir Simpson Category 1+ (i.e. excluding Tropical Storms), Middle: CNRM climate model- Future STORM track density, of Saffir Simpson Category 1+, and Right: The cyclone track density difference between them.

2.2.2 Hydrodynamic model implementation

The first requirement before running baseline and future simulations in the MIKE 21 FM model is to import the sub-set of STORM-derived TC data, into the MIKE 21 Cyclone Wind Generation toolbox. The data for each individual TC was formatted using a MATLAB script to process the input data (wind speed, radius to maximum winds and track coordinates) and generate a MIKE 21 wind/pressure forcing file. As before we utilised the Single Vortex Holland option, with the Holland B parameter estimated using the Holland Formula specified in Harper and Holland (1999). The resulting outputs ~94,100 total MIKE 21 FM cyclone wind/pressure files (~30,800 baseline and ~63,300 future) were generated at a 0.25 degree x 0.25 degree resolution, with a timestep of 3-hours. This spatial resolution was sufficient to resolve the TC within these forcing files, especially as the wind/pressure files would be further interpolated in the MIKE 21 FM software to the higher resolution of the model mesh as the cyclone traverses through the model domain.

MATLAB scripts were also used to create associated steering (control) files. The steering file differentiates the parameters of each simulation, by for example pointing to the next cyclone wind/pressure file or by generating a unique output filename. These steering files define the model solution technique, to integrate the time and space variables within the shallow water equations via an explicit scheme, utilising a variable time step interval in the calculation. The critical CFL number was set to 0.8 in the steering file. The recommended default Manning number (i.e., 32 $m^{1/3}s^{-1}$) was used to define bed resistance over the entire domain. The steering files were set up so that each model simulation starts at the timestep at which the synthetic cyclone started or entered the grid

domain, and terminates the run at the time-step the cyclone exited the domain or dissipated. Time-series results were set to export at a 10-minute temporal resolution for each simulation.

For reasons of data economy, we chose to only save (output) predicted surge time-series at discrete points for each simulation, rather than across the 13,350 nodes of the entire grid domain. These discrete 3,051 output coastline points (OCP) are located along the length of the Chinese, Vietnamese, Cambodian and Thai (and half of Malaysian) coastlines in the model, at separation distance of approximately 2 km to 5 km (OCP are shown as green in Fig. 1a).

Before running the models, we checked if non-linear interactions between the tide and non-tidal components would influence model output of still total water level levels in this region (Idier et al., 2019; Horsburgh and Wilson, 2007). Flood hazard can be underestimated if these non-linear interactions are not accounted for (Arns et al. 2020; Williams et al., 2016). We determined that the differences in the height and duration of storm surge is negligible, with only the timing of the surge peak nominally impacted between high and low water tidal states (see supplementary material section 3). As a result, we implemented all model simulations as meteorological forcing only ('surge-only'). The final step was therefore to run each MIKE 21 model on the University of Southampton's IRIDIS 5 High Performance Computing Facility. On average, each simulation took around 15 minutes to complete.

2.2.3 Computation of return periods

Upon completion of all the simulations, each OCP has estimated surge levels from a very large number of individual cyclone passes, for both the baseline (1980-2018; ~30,800 cyclones) and future (2015-2050; ~63,300 cyclones) model scenarios. These number of model outputs represent a synthetic record of 10,000 years of TC activity, for each of the baseline and future periods, and allows for a robust estimation of even extreme return period levels (RPL) at every OCP. In estimating these RPLs, we employed the following methodology: (i) the annual surge maxima was found for every one of the 10,000 years of the synthetic record, for each OCP (since each TC in the STORM database has a given synthetic month and year. There may be 2-15 TCs making landfall within our domain area each STORM year); (ii) these maxima surge levels were then sorted in descending order and given a rank (m) before; (iii) the probability of exceedance (P) was calculated using the Gringorten formula:

$$P = \frac{(m-a)}{(n+2a)} \quad (1)$$

where a is scale parameter equal to 0.44, n is the number of extreme values. The RPL therefore is given as 1/P. The Gringorten formula was used due to its suitability for extreme value estimation (irrespective of sample size) and past record in unbiased return period estimation (Guo, 1990).

In addition to calculating surge-only return periods as described above, we also estimated total still sea level return periods for each OCP. Because non-linear interactions between tide and non-tidal components were determined to not be an issue for this region, we do this by adding surge levels to a semi-randomly selected tide. The first step to calculate total still sea levels was to run a tide-only model simulation (for the year 2009 where we had already obtained OTIS tide data) and to save modelled tide levels at each of the OCPs at 10-minute intervals. We then secondly input this year of detailed tide levels into the MATLAB T-Tide script (Pawlowicz et al., 2002) to obtain

the tidal constituents and predict the tides over a longer recent 19-year period (2003 to 2021). A full 19-year period was targeted because it encompasses a complete 8.85-year cycle of lunar perigee and covers the 18.6-year nodal astronomical tidal cycle, both of which can influence extreme sea levels (Baranes et al., 2020; Peng et al., 2019; Haigh et al., 2011). The third and final step was to select a semi-random date from this 19-years of tide data that would match with a TC in the baseline and future datasets. The original past/present and future STORM datasets has TCs develop largely between May and November, as occurs in the natural record for this region. Our sub-sets of baseline and future TC data, derived from STORM, all have a simulated month and synthetic year assigned to them. Because of this it was possible to match each TC (surge) to the correct month in the tide data, preserving TC seasonality. We subsequently could allocate a random time, day and year from the 19-year tidal cycle. This produces an appropriate surge + random tide result from which to estimate baseline or future extreme sea levels, and then to calculate total RPLs using the same method described above for surge-only RPLs.

Our approach is not without uncertainty, particularly for the most extreme (1,000 year) RPLs. Therefore, this RPL estimation process was repeated 100 times in a Monte Carlo approach, providing 100 return level estimates for each OCP. The mean of these 100 RPLs was then selected. Either a peaks over threshold or annual maxima method could have been employed for statistical estimation of RPLs. However, because our interest is in selecting surge peaks (TC events) which are independent of one another, and it is not known if the assumption of complete TC independence in the STORM datasets is valid, we selected the annual maxima approach, since 10,000 years of data is plentiful.

3 Results

We now present the results of our approach. Storm surge-only results are presented first in section 3.1, and then in section 3.2 we show results accounting for other influences on sea level (tides and absolute mean sea-level rise).

3.1 Extreme storm surge return period levels

First, we focus on the surge-only return period levels. Figure 6a,b,c illustrate the computed 10% AEP (1:10 year), 1% AEP (1:100 year) and 0.1% AEP (1:1000 year) RPLs respectively, for the baseline (1980-2018) scenario. In the middle row, Fig. 6d,e,f illustrates the same 10% AEP, 1% AEP and 0.1% AEP RPLs, for the future period (2015-2050). In the baseline scenario (Fig. 6b,c : top row) we see that RPLs are slightly higher along the Chinese coastline, reflecting the more frequent cyclone activity in this region of the model domain (Fig. 5a), with the peak 1% AEP surge-only RPL reaching 3.5 m at one OCP here. The shape of the coastline has a strong modulating effect on surge height, that is especially noticeable for the more extreme events, whereby the modelled surges are typically amplified within the many bays, river mouths and inlets located along this northern coastline (Jelesnianski, 1972). Another effect of the shape of the shore is seen along the Vietnam central coastline, where surge RPLs are substantially lower (1% AEP is ~0.3 m) compared to the coastlines of north and south Vietnam. The narrow width of the continental shelf in central Vietnam reduces surge amplitude; behaviour that is noticeable even for the most extreme surges (Fig. 2 & 1b; Fig. 6b,c). The correlation between storm surge height and continental shelf width is a well-documented characteristic (Pugh and Woodworth, 2014).

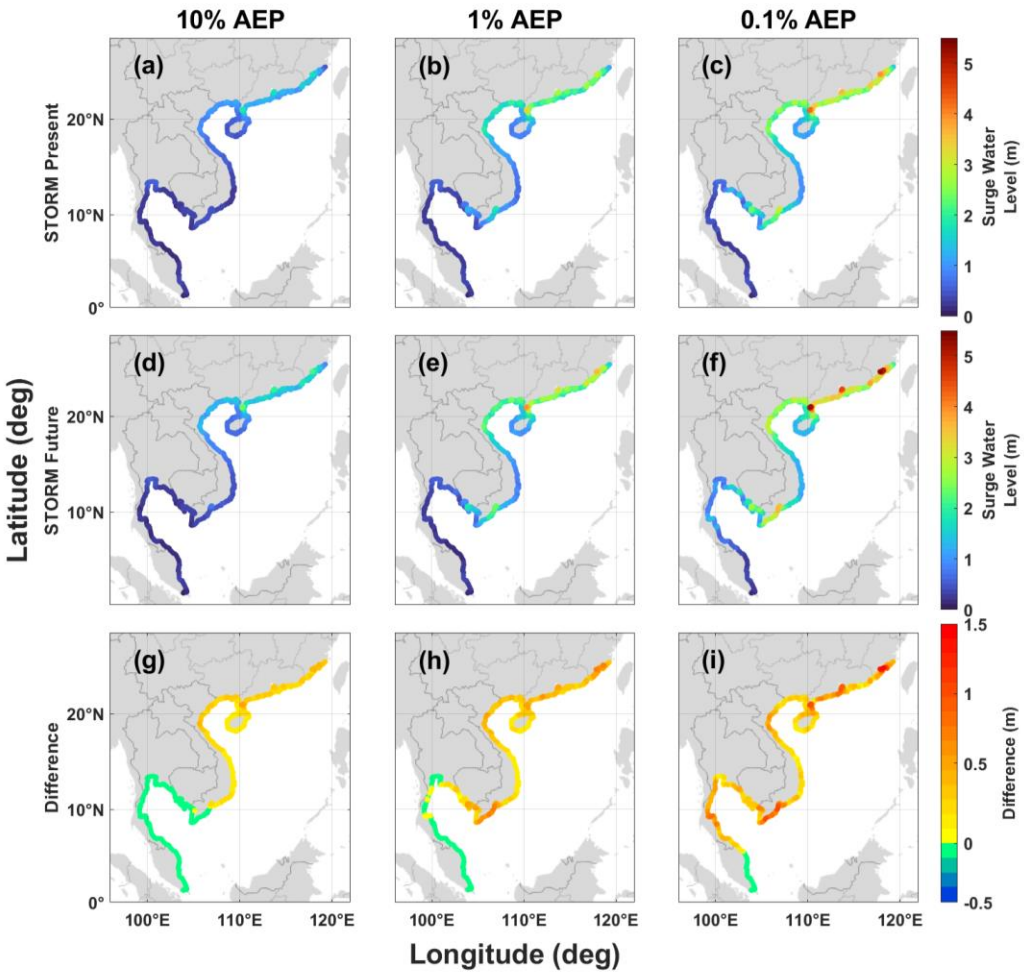

Figure 6 - The 10% AEP (a,d,g), 1% AEP (b,e,h) and 0.1% (c,f,i) AEP return period sea levels (surge-only) for the China, Vietnam, Cambodia, Thailand and Malaysian coastlines in the model, using first row: STORM baseline data (1980-2018), second row: CNRM climate model STORM Future data (2015-2050), third row: a difference plot to highlight the areas with greatest change in surge level between STORM baseline and STORM future model results.

In the middle row of Fig. 6, illustrating the future scenario, we see that surge levels have increased substantially, over the timescale, in height and extent between China and Malaysia. The future 1% AEP RPLs in Fig. 6e for example, show that the length of coastline that is exposed to storm surge levels of 2.5 m (95th percentile storm surge level) or greater more than doubles in length by 2050, going from 353 km to 930 km total length. Over our time period, extreme RPLs are extending from Chinese coastlines into parts of north and south Vietnam. Similarly, comparing the extreme 0.1% AEP scenario, there is approximately 231 km of mostly Chinese coastline that we estimate currently has 3.5 m (~95th percentile storm surge level) or greater storm surge heights (Fig. 6c). This length increases in extent to around 577 km of coastline with future TCs conveying these highest storm surges also into north and south Vietnam (Fig. 6f).

Again contrasting baseline and future surge levels, in the difference plots of Fig. 6 bottom row, we see that the greatest 1% AEP level increase is approximately 0.8 m around the south Vietnam coastline (Fig. 6h). The greatest 0.1% AEP level increase is around 1.6 m along the Chinese coastline (Fig. 6i). The shape of the coastline, specifically a wide and gently sloping continental shelf and the angle of cyclone approach contribute to this amplification of the more extreme RPLs around these particular coastlines, notably including around the more

vulnerable Red and Mekong River deltas in Vietnam (Fig. 2; Ramos-Valle et al., 2020; Pandey and Rao 2019; Bloemendaal et al., 2019b; Poulose et al., 2018).

Looking beyond China and Vietnam, the baseline model outputs indicate that the coastlines of Cambodia, Thailand and (partially) Malaysia are currently relatively unaffected by storm surges linked to lowest category TCs, storms and depressions. This is expected, as these coastlines have historically rarely experienced cyclone induced storm surges of magnitude (>10% AEP). And for more probable storm surge events up to the 10% AEP level, this status is predicted to continue into the future too (Fig. 6d). Present-day 10% AEP storm surge heights along these coastlines average around 0.36 m - and between today and mid-century there appears to be zero increase in levels. However going to more extreme storm surge probabilities by the year 2050, sections of this coastline are projected to experience storm surges up to 0.6 m (1% AEP) and 0.8 m (0.1% AEP) higher than current levels (Fig. 6h,i). In some locations this doubles the current (baseline) storm surge heights.

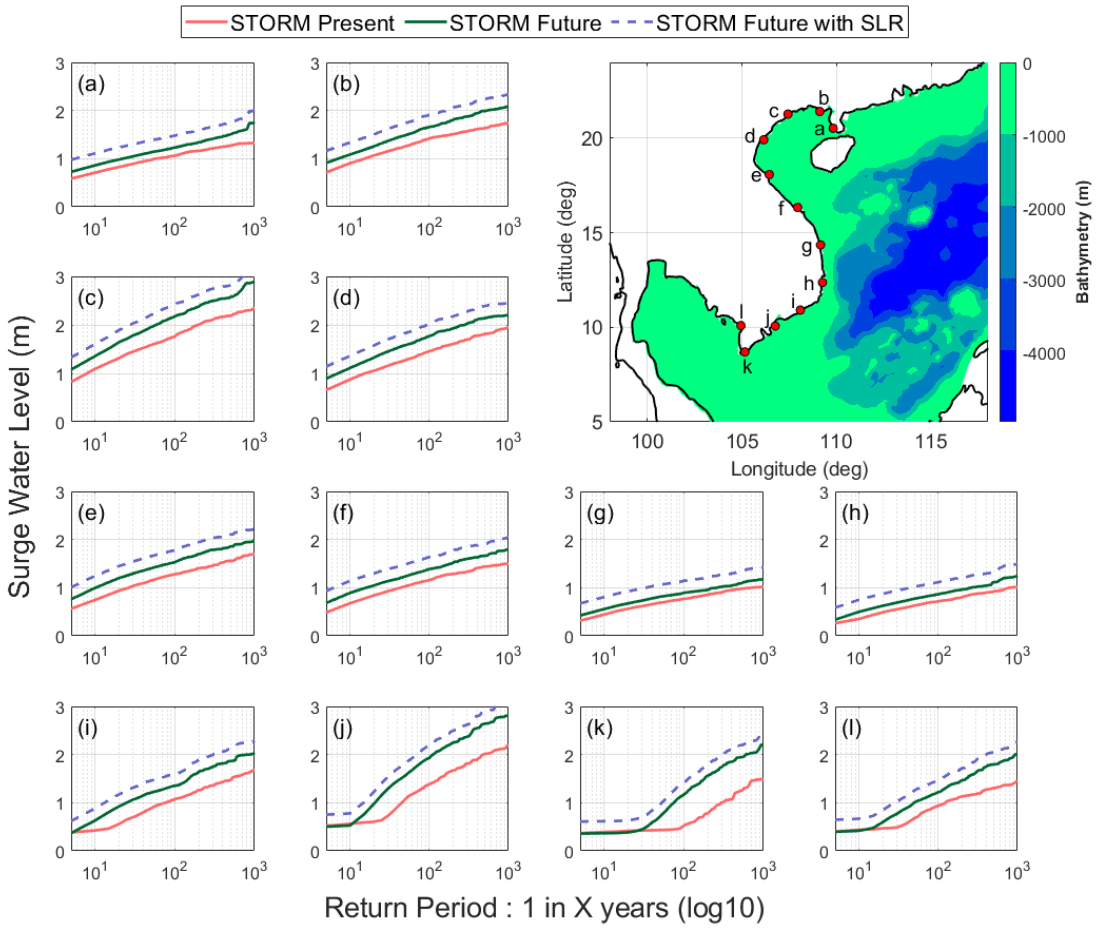

Figure 7 - The relationship between synthetic baseline (pink) and future (green) 'surge-only' return period sea levels (Log scale, 1:X years) at equidistant locations at and around the Vietnam coastline. Future return periods with 0.25 mean sea-level rise (SLR), due to climate change by 2050, is shown with a dashed blue line.

Given the above interesting and varying results for north to south Vietnam coastlines, we display in Fig. 8 surge RPLs for 12 equidistant discrete OCPs, along this coastline. Figure 7 illustrates two things. The first relates to coastal morphology – this show that storm surge RPLs are lowest around the central Vietnam coastline (points g,h), where the narrow continental shelf acts to reduce surge amplitude. In both baseline and future scenarios

within this central zone, the difference between the smallest (20% AEP, 1:5 year) and largest (0.1% AEP, 1:1000 year) RPLs is less than 1 m. This suggests that the amplitude-dampening effect provided by the coastal morphology extends to even the most severe storm surges. The second thing relates to rate of growth in storm surges over time – the vertical distance between baseline and future sea levels. It is possible to see that the largest growth in modelled storm surge heights over the next 30 years can be found in the southern part of Vietnam. The future 1% AEP storm surge near to the Mekong River delta (points j,k) for example is average 0.6 m higher than the current ~1 m storm surge value, while at the northern coastline of Vietnam near to the Red River delta (point d), the storm surge difference is only around 0.3 m. It is half this again at around 0.12 m difference for the same 1% AEP return period in the sheltered central zone (points g,h).

3.2 Extreme total water level return period levels

Representative total still sea levels (surge + tide) for the 10% AEP, 1% AEP and 0.1% AEP return period events for both the baseline and future scenarios are shown in Fig. 8. A comparison against the surge-only results in Fig. 6 shows that the addition of tides increases the sea level height by as much as a further 2 m along the Chinese coastline, the Gulf of Tonkin, south Vietnam and southern Thailand. Elsewhere tides add between 0.3 m and 1 m to surge levels.

In southern Vietnam, the mean present-day 1% AEP total water level is modelled at approximately 1.9 m above mean sea level (amsl), but by 2050 the 1% AEP mean total water level would be approximately 2.2 m amsl; an increase of 0.27 m over the intervening ~30 years. Similarly, in northern Vietnam, where the Red River delta is located, the baseline 1% AEP mean total water level is approximately 2.1 m amsl and by 2050 this would increase to approximately 2.4 m amsl. The corresponding increase between the more extreme 0.1% AEP baseline and future mean total water levels is estimated to be around 0.36 m in the north, and 0.56 m in the south of the country.

In addition to extreme total water levels from TC-induced storm surges and tides, the South China Sea area will also experience mean sea-level rise by the middle of this century (absolute sea-level rise – i.e. ignoring other factors such as land subsidence). The IPCC's 6th Assessment Report estimate of projected mean total sea-level rise (relative to a 1995-2014 baseline) along the coastline of Vietnam is 0.25 m by the year 2050, under the SSP5-8.5 reference scenario (NASA sea-level tool: https://sealevel.nasa.gov/ipcc-ar6-sea-level-projection-tool). Figure 8g-i shows the 10% AEP, 1% AEP and 0.1% AEP return period with 0.25 m of mean sea-level rise simply added (we ignore any indirect effects). Adding a mean sea-level rise to the future 1% AEP mean total water levels takes these levels to approximately 2.7 m amsl for the north of the country and 2.4 m amsl around the south. What is notable in Fig.s 7 to 9 is that by 2050, along many points on the Vietnam and Chinese coastlines, the scale of increase in storm surge regularly surpasses the 0.25 m size of projected sea-level rise. This holds true for 1% AEP return periods, and the magnitude of the effect increases as events become more extreme (up to 0.1% AEP). The exception to this result is at the central coastline of Vietnam where surge amplitudes are consistently reduced, even at extreme probabilities, as discussed previously.

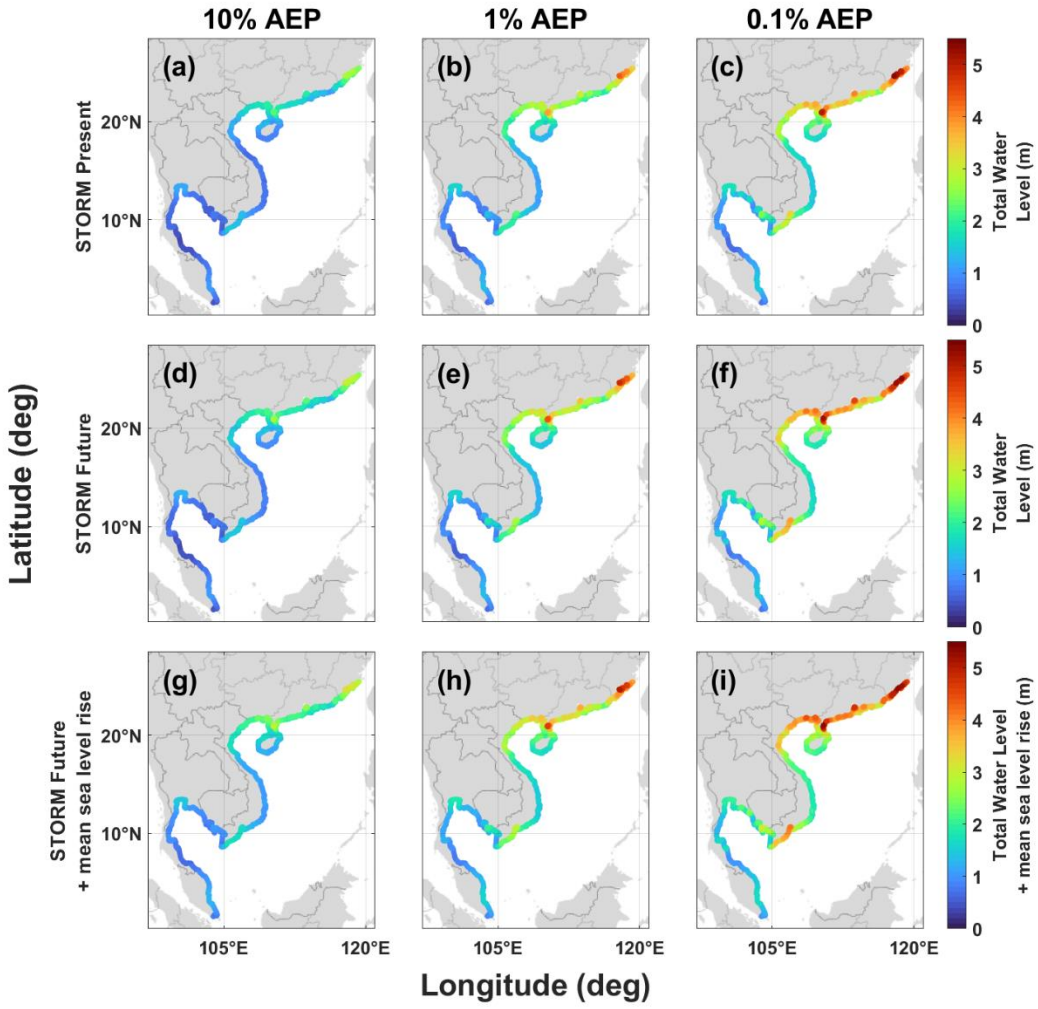

Figure 8 - The 10% AEP (a,d,g), 1% AEP (b,e,h) and 0.1% (c,f,i) AEP return period total water levels (tide + surge) for the China, Vietnam, Cambodia, Thailand and Malaysian coastlines in the model, using first row: STORM Baseline data (1980-2018), second row: CNRM climate model STORM Future data (2015-2050) total water levels, third row: CNRM climate model STORM Future data total water levels with 0.25m addition for rising mean sea levels along Vietnam coastline by 2050.

3.3 Cyclone tracks

As a side point of interest, we include an illustration of how the orientation and strength of cyclones varies by location, using our baseline simulation results. Figure 9 shows the track of the synthetic cyclones responsible for the 10 largest modelled surges at 12 random equidistant point located along the coastline of Vietnam and China. There are clear differences, moving geographically north to south, in the origins and magnitudes of each cyclone. But what they all have in common is they pass to the south/west of each point as the TCs travel westwards within the domain. This is expected, as the Coriolis effect pushes winds in a cyclonic (counter-clockwise) direction in the northern hemisphere, and it is the strong onshore winds in the first and second cyclone quadrants that are responsible for generating a large part of the storm surge.

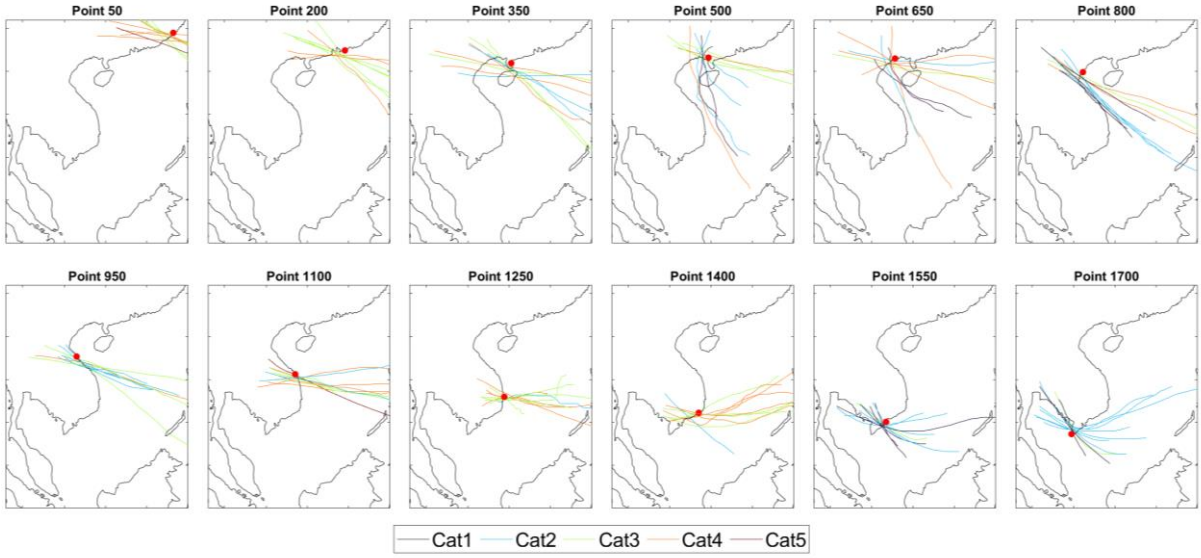

Figure 9 – The tracks of the baseline STORM cyclones which produce the 10 largest surges at randomly selected OCP points along the Vietnam and China coastlines. All demonstrate that it is the onshore winds associated with the cyclone that are forcing storm surge levels. Before around point 1700 a counter-clockwise-turning TC travelling westwards ensures that onshore winds (and thus storm surges) were north-east of TC, and offshore winds south-west. However after this point, with the coastline turning, onshore winds flip around so that storm surges and onshore winds are south-west of TC, with offshore going winds north-east.

4 Discussion

We forced a hydrodynamic coastal model of the South China Sea with databases of present and future TC activity, to gain a better understanding of the potential changes to storm surge and extreme sea level behaviour over the next thirty years, due to projected climate change in this region. This area of south-east Asia is considered to be a 'hotspot' for projected future sea level extremes related to intense TC storm activity (Nicholls et al., 2021; Kirezci et al., 2020; Nicholls and Cazenave, 2010; McGranahan et al., 2007). One facet of this change suggests that a trend of TCs gradually migrating polewards and achieving their maximum intensity in more northern latitudes is expected to continue into the future (Kossin et al., 2014). This trend is in fact seen in the CNRM-CM6-1 global climate model behind the STORM data used in this analysis, along with an apparent greater number of more intense TCs occurring in the future within the WNP region. Within the smaller limited domain of our South China Sea model, we also see projected a wider distribution of activity over this region, with an increasing number of strikes to eastern coastlines (particularly central Vietnam), and even a small number of TCs travelling further southwards. The reasons were not explored but could be a seasonal effect; recent research suggests that peak season (July-September) TCs in the WNP are more likely to migrate polewards than later-season (October-December) TCs (Feng et al., 2021).

When we forced our South China Sea coastal model with synthetically generated TCs from STORM (Bloemendaal et al., 2022 & 2020), our results showed that this projected shift in TC behaviour over time would raise surge heights along lengths of the Chinese and Vietnamese coastlines (Fig. 6). By 2050, storm surges along Chinese and Vietnamese coastlines may be up to 0.8 m (1% AEP; 1:100 year) and 1.6 m (0.1% AEP; 1:1000 year)

higher than today. Of course, TC approach angle means that some north and eastern stretches of coast in the model domain (Fig. 2) would be orientated to be more vulnerable to storm surges, irrespective of their coastal morphologies, because of funnelling effects within bays and inlets (Pandey and Rao, 2019). However, coastal morphology can modulate surge heights in certain instances too. Despite storm surge heights increasing along the Vietnamese coastline by 2050, future storm surges along the central portion of Vietnam's coastline are actually smaller than neighbouring levels to the north and south (Fig. 6 & Fig. 7). Even though this section of coastline is most exposed to increases in the frequency and intensity of TCs that induce storm surges (Fig. 5c). Surge heights are modulated here because there is no wide and gently sloping continental shelf to amplify storm surge energy, and there are few coastal inlets and river mouths here to funnel and enhance storm surge wave heights (Dube et al., 1981; Jelesnianski, 1972).

The model has a variable triangular grid resolution, with greater detail along coastlines. It should be noted that there is potential for sub-optimal accuracy in storm surge levels, particularly within small coastal features such as inlets, bays or estuaries, where coastal resolution is insufficient to capture features in detail. For example, Bertin et al. (2015) showed that within small seas wave radiation can induce set up that transforms storm surge levels along exposed coastlines, with even the small waves entering bays and inlets affecting water levels. Unfortunately, the number of TC simulations entailed in this study meant that there had to be a trade-off between rendering coastal detail and reasonable computation timescales. Future work in such locations, looking at local sections of coastline, would require detailed modelling to estimate extreme sea levels due to storm surge. Additionally, currents and wave action is specifically not incorporated in the modelling as it was outside of the project scope. Such wave models will be a valuable addition to the scientific discussion, as their high spatial resolution at the coastline would ensure that nearshore wave dynamics, such as wave setup, are adequately resolved (Hinkel et al., 2021; Saulter et al., 2017).

Beyond the increased storm surge heights along northern Vietnam and China, our results suggest that the effects of a changing climate on extreme sea levels will also effect more southerly latitudes around southern Vietnam, Cambodia and Thailand. This is troubling as currently extreme sea levels here are rare events. The modelled 10% AEP surge heights presently averages around 0.36 m along this Vietnam-Cambodia-Thailand portion of coastline. The more extreme 1% AEP storm surge rarely exceeds 0.5 m along these coastlines, and there is so little storm surge activity that for some sections of Thailand and Malaysia coastline the difference between 10% AEP and 0.1% AEP extreme sea levels is under 10 cm. Over the next thirty years we found that the lowest-impact/highest probability storm surges (>10% AEP) along these coastlines are unlikely to greatly increase. However, more extreme storm surges (1% AEP to 0.1% AEP) do begin to increase in size due to a changing climate over this same timescale (Fig. 6). The worst hit sections of Vietnam-Cambodia-Thailand coastline see 1% AEP storm surge heights increase by 0.6 m (0.8 m for 0.1% AEP surges). The implications of this is that the flood defences and plans for these previously sheltered coastlines may over time become unfit for purpose, as a consequence of the projected climate changes in this region leading to TC-induced storm surges.

We also examined what happens to storm surge frequency with TCs occurring with greater intensity in the future. The gap between baseline and future RPLs in Fig. 7 suggests that the extreme storm surge levels we experience today, would in the future occur with greater regularity. For example, a 1% AEP storm surge occurring around point j (near Ho Chi Minh City) with height of ~1.4 m today (excluding tide and mean sea-level rise contributions),

is projected to occur at close to 2.8% AEP (1:35 year) frequency by the year 2050. Storm surge levels associated with a 1% AEP event near to the Red River delta (point d) today would correspond to a 3.3% AEP (1:30 year) frequency by 2050. The same effect can be observed to varying degrees for all location points plotted, with greater increase in occurrence observed in the north/south parts of Vietnam coastline (points a-f and i-l) than observed in the middle section of coastline (points g-h). This substantial increase in frequency suggests that flood defence standards will need to be upgraded at coastal locations and flood managers will need to consider augmented, alternative or combined methodologies to cope with more widespread, higher or more frequent storm surge scenarios. Complex and higher dyke systems alone may be insufficient for storm surge flood hazard. It's also worthwhile considering that breaches in storm surge defences may coincide/combine with pluvial runoff or fluvial flooding after a typhoon or monsoonal rainfall when normal inland flood releases (e.g. drains, flood gates or flood storage areas) could be unavailable.

A greater number of intense TCs in the future due to projected climate changes, more spatially dispersed than today, means not only that extreme sea levels become higher in the future, but that the total lengths of coastline experiencing the more extreme storm surges extends also. In our analysis, the highest storm surge levels (≥ 2.5 m in 1% AEP, ≥ 3.5 m in 0.1% AEP: approximately the 95th percentile of OCP storm surge levels) seen today occurring only along the coastline of southern China, are projected to extend further south into Vietnam over the next 30 years. This spread would more than double the length of coastline currently impacted by such high surge levels (Fig. 6). In Vietnam, the northern communes have more experience of TCs making landfall with some regularity and bringing TC-induced storm surges. The system of flood defences is better prepared for such eventualities. But at Vietnam's southern coastlines the population is not as well-equipped to withstand extreme sea level inundation (Anh et al., 2017; Larson et al., 2014; Takagi et al., 2012; Kleinen 2007). A significant proportion of the country's total population lives along this low-lying coastline in cities or within its two main deltas; the Red and Mekong River deltas (Nicholls et al., 2021; Bangalore et al., 2019; GFDRR., 2015; Hinkel et al., 2014; Dasgupta et al., 2009). This alongside the considerable agricultural and infrastructure capital value, explains why these low-lying coastlines have particular vulnerability to storm surges hazard (Edmonds et al., 2020; Hung et al., 2012; Nguyen et al., 2007). The Mekong River delta has long been identified as being at particular risk of coastal flooding because mean sea levels have been historically rising here at the same time that mean land elevations have been sinking and sinking at a faster rate than previously realised (Nicholls et al., 2021; Oppenheimer et al., 2019; GSO, 2019; Minderhoud et al., 2017; Dang et al., 2018; Erban et al., 2014; Hung et al., 2012). As one of the most strategically important areas of the entire model domain, we aim to explore the potential impacts of predicted extreme total water levels to the Mekong River delta region in a future paper.

Mean sea-level rise has not been explicitly incorporated in our future model simulations, but it would likely have an amplifying effect on extreme sea levels. To accommodate the impact of mean sea level rise for the Vietnam coastline as an example, we instead simply added a standard 0.25 m increase on top of total water level results for Fig. 7. Having a somewhat greater sea depth could act to slightly reduce the energy of a storm surge wave at the coastline. Even so, a small additional height of water on top of storm tide levels in the final trade-off may be enough to extend inundation area or overtop carefully designed flood defences. Relative and regional sea-level rise should therefore always be considered in coastal flood emergency strategies. It is worthwhile noting that the projected increases in storm surge heights along the entire Vietnamese coastline over the next 30 years, ranges up to 0.7 m in the 1% AEP (and up to 1 m in the more extreme 0.1% AEP). But even an average of all 1% AEP surge

level increases along this coastline actually exceeds the anticipated permanent addition due to climate change on local sea levels. Consequently, storm surge would appear to present a bigger (albeit limited-time) hazard to this region than rising mean sea levels, by 2050. This is particularly interesting, as past changes in mean sea-level have dominated changes in extreme sea levels in extra-tropical regions, with mostly negligible changes observed in storm surges (Mawdsley and Haigh 2016; Marcos et al., 2015; Seneviratne et al., 2012).

The results of our study, which highlights the large - and growing - impacts of storm surge flooding, clearly demand an urgent re-evaluation of existing flood risk, defence design and planning standards to include appropriate focus on the emerging risks posed by climate driven storm surges. High value areas south of around 15 degrees latitude which have historically disregarded the risks posed by current and future storm surges, have the strongest exposure to this risk (Anh et al., 2017; Takagi et al., 2012).

There are factors that influence extreme sea levels (such as wave run up and set up, TC latitude or seasonality of mean sea level) that have not been incorporated in our model set up as they are currently beyond the scope of the project. However, they could easily be incorporated in future analysis. For example, we constructed TCs for the MIKE 21 model using the Holland method (Harper and Holland, 1999), but alternative approaches may produce slightly different TC wind and pressure gradients in the model to induce storm surge heights. Naturally, there are also alternative choices that could have been made in our study approach that would or may have altered our findings. For example, we selected a single future STORM scenario (CNRM-CM6-1) out of a possible four climate model outputs and any biases in this data would also translate into our model results. However, all STORM versions of the averaged 2015-2050 future climate (Table 3) consistently showed an increase in TC intensity, frequency and altered spatial distribution in the South China Sea region. Future work could compare results across the other three simulations to better quantify uncertainty.

Additionally, the choice of a future STORM scenario which uses a mean SSP5-8.5 profile to indicate the extent of future TC's may be a limitation of our study as this projected future climate has the highest greenhouse gas emissions between 2015-2050, assuming only limited climate change mitigation measures globally over the next 30 years. This choice may therefore overestimate current greenhouse gas trajectories (e.g., Hausfather and Peters, 2020) compared to other SSP scenarios. Moreover, while it is a benefit of the global climate models used in future STORM that they run with a high spatial resolution, because this nicely resolves individual TCs, this does require a trade off against computational costs so that only the period up to 2050 could be produced by Bloemendaal et al. (2022). Should this detail change and future STORM simulations are extended out to 2100, it would be interesting to rerun the hydrodynamic model simulations for this longer time period.

5 Conclusions

As the latest IPPC report has indicated, there is little (~20%) confidence in the scientific community being able to accurately predict future changes to storm surge characteristics, particularly in the sparsely gauged regions of the world exposed to tropical cyclones (TC). Statistical and numerical models have improved our knowledge in this subject area regionally and globally. However, in tropical regions where TCs are most actively creating storm surges, such as the South China Sea, coarse hydro-meteorological data and scarce tide gauge observations often limit progress. To address this problem, we utilised two newly available databases, each of 10,000 years of

synthetic TC track data, created by Bloemendaal et al., (2020; 2022). The STORM databases cover both a past period and the SSP5-8.5 future realisations to the year 2050. We created a bespoke hydrodynamic model of the South China Sea region to simulate 10,000 years of TC activity on sea level, for present (baseline) and projected future SSP5-8.5 climate conditions. We estimated the projected impact of TCs on storm surge heights alone, and also on extreme total water levels (surge + tide).

The model results show that extreme sea levels powered by storm surges will increase substantially in the near future for many sections of this coastline. Today's extreme sea levels will be a more common occurrence by 2050; for example, a 1% Annual Exceedance Probability (AEP, 1:100 year) storm surge today will likely be experienced with a frequency closer to 5% AEP (1:20 year) in thirty years' time in some locations. And as TC activity in this region increases and expands geographically over time, so does the spatial extent of extreme sea levels forced by storm surges. We predict that the coastlines of China and North and South Vietnam will experience a greater increase in storm surge heights than elsewhere in the model domain. In a 1% AEP (1:100 year) event, storm surges could increase up to 0.8 m over present day heights. We found that the length of coastline experiencing today's highest (95^{th} percentile) storm surge levels of ≥ 2.5 m (1% AEP) or ≥ 3.5 m (0.1% AEP) more than doubles over the next thirty years. But in contrast, the coastline of central Vietnam has more natural resilience against present and future storm surges because the adjacent narrow continental shelf limits surge growth even with stronger forcing.

In the present climate, the coastlines of Thailand and Cambodia hardly ever experience significant TC storm surges. However, these countries are projected to experience changes to storm surge with more intense TCs striking sections of their coastlines over the next thirty years. Our simulations predict that, for the first time, these coastlines will experience storm surge levels above 0.5 m in the extreme RPLs (≥1% AEP). Flood management approaches along these regional coastlines will therefore need to be reviewed for their effectiveness against future extreme sea levels and storm surges.

Lastly, our results show that the difference between extreme storm surge heights today and those by year 2050, along the coastlines of Vietnam and its neighbours, regularly exceeds the 0.25 m SSP5-8.5 scenario mean sea-level rises projected for this region. Climate-driven changes in storm activity in this tropical zone will produce higher extreme sea levels, and enhance storm surge hazard, that in many locations will present a greater challenge for coastal flood management over the next decades than will mean sea-level rise alone.

Author contribution

MW carried out the hydrodynamic modelling simulations, formal analysis and prepared the first draft of the manuscript. IDH, SED and RJN conceptualised this work, designed the methodology and provided supervision in the UK. IDH further supervised model design and visualization. The supervision, methodology development and resources in Vietnam were provided by TBH and NNH, with formal data analysis carried out by QQL. NB provided key tropical cyclone resources for this study. All authors commented and edited the manuscript prior to submission.

Competing interests

The authors declare that they have no conflict of interest.

Acknowledgements

This work was supported by the Natural Environment Research Council, in the UK (Grant Number NE/S003150/1). Also supported in Vietnam by the National Foundation of Science and Technology Development (NAFOSTED-RCUK fund) and with data from the Ministry of Science and Technology of Vietnam's river training solutions of the Mekong River project (code DTDL-48/18).. The authors also wish to acknowledge the use of the IRIDIS High Performance Computing Facility, and associated support services at the University of Southampton, in the completion of this work. Lastly, this work could also not have been completed without access to the STORM present and future datasets (Bloemendaal et al., 2022). NB is funded by a VICI grant from the Netherlands Organization for Scientific Research 569 (NWO Grant Number 453-13-006) and the ERC Advanced Grant (Grant Number COASTMOVE 884442).

References

Anh, L.T., Takagi, H., Thao, N.D. and Esteban, M., Investigation of awareness of typhoon and storm surge in the Mekong Delta–Recollection of 1997 Typhoon Linda, Journal of Japan Society of Civil Engineers, Ser.B3 (Ocean Engineering). Vol. 73(2), pp.I_168-I_173, 2017.

Arns, A., Wahl, T., Wolff, C. et al., Non-linear interaction modulates global extreme sea levels, coastal flood exposure, and impacts, Nat Commun. 11, 1918, https://doi.org/10.1038/s41467-020-15752-5, 2020.

Bangalore, M., Smith, A. and Veldkamp, T., Exposure to floods, climate change, and poverty in Vietnam, Economics of Disasters and Climate Change volume 3, p79–99, https://doi.org/10.1007/s41885-018-0035-4, The World Bank, 2019.

Baranes, H.E., Woodruff, J.D., Talke, S.A., Kopp, R.E., Ray, R.D. and DeConto, R.M., Tidally driven interannual variation in extreme sea level frequencies in the Gulf of Maine, Journal of Geophysical Research: Oceans, 125(10), p.e2020JC016291, 2020.

Bertin, X., Li, K., Roland, A., Zhang, Y.J., Breilh, J.F. and Chaumillon, E., 2014. A modeling-based analysis of the flooding associated with Xynthia, central Bay of Biscay. Coastal Engineering, 94, pp.80-89.

Bloemendaal, N.; Haigh, I.D., de Moel, H. ; Muis, S, Haarsma, R.J., Aerts, J.C.J.H., STORM IBTrACS present climate synthetic TROPICAL CYCLONE tracks, 4TU. Research Data, Dataset. https://doi.org/10.4121/12706085.v3, 2019a.

Bloemendaal, N., Muis, S., Haarsma, R.J., Verlaan, M., Apecechea, M.I., de Moel, H., Ward, P.J. and Aerts, J.C., Global modeling of tropical cyclone storm surges using high-resolution forecasts, Climate Dynamics, 52(7), pp.5031-5044, 2019b.

Bloemendaal, N., Haigh, I.D., de Moel, H., Muis, S., Haarsma, R.J. and Aerts, J.C., Generation of a global synthetic tropical cyclone hazard dataset using STORM, Scientific Data, 7(1), pp.1-12, 2020.

Bloemendaal, N., de Moel, H., Martinez, A. B., Muis, S., Haigh, I. D., van der Wiel, K., Haarsma, R. J., Ward, P., Roberts, M. J., Dullaart, J. C. M., & Aerts, J.. A globally consistent local-scale assessment of future tropical cyclone risk. Science advances, 8(17). 2022.

Calafat, F.M., Wahl, T., Tadesse, M.G. and Sparrow, S.N., 2022. Trends in Europe storm surge extremes match the rate of sea-level rise. Nature, 603(7903), pp.841-845.

Caldwell, P. C., Merrifield, M. A. Thompson, P. R., Sea level measured by tide gauges from global oceans - the Joint Archive for Sea Level holdings (NCEI Accession 0019568), Version 5.5, NOAA National Centers for Environmental Information, Dataset, doi:10.7289/V5V40S7W, 2015.

Chan, J.C., Interannual and interdecadal variations of tropical cyclone activity over the western North Pacific, Meteorology and Atmospheric Physics, 89(1), pp.143-152, 2005.

Cid, A., Camus, P., Castanedo, S., Mendez, F., & Medina, R., Global reconstructed daily surge levels from the 20th Century Reanalysis (1871-2010), Global and Planetary Change, 148, 9-21, 2017.

Cid, A., Wahl, T., Chambers, D., & Muis, S., Storm Surge Reconstruction and Return Water Level Estimation in Southeast Asia for the 20th Century, Journal of Geophysical Research, 123(1), 437-451, 2018.

C3S (Copernicus Climate Change Service), ERA5: Fifth Generation of ECMWF Atmospheric Reanalyses of the Global Climate, https://cds.climate.copernicus.eu/, 2020.

Dang, T.D., Cochrane, T.A. and Arias, M.E., Future hydrological alterations in the Mekong Delta under the impact of water resources development, land subsidence and sea-level rise, Journal of Hydrology: Regional Studies, 15, pp.119-133, 2018.

Dasgupta, S., Laplante, B., Meisner, C., Wheeler, D. and Yan, J., The impact of sea-level rise on developing countries: a comparative analysis, Climatic change, 93(3), pp.379-388, 2009.

DHI. MIKE 21 Flow Model - Hydrodynamic Module, User Guide, https://manuals.mikepoweredbydhi.help/latest/Coast_and_Sea/M21HD.pdf, 2017a.

DHI. MIKE 21 Flow Model – Cyclone Wind Generation Tool. Scientific Documentation, https://manuals.mikepoweredbydhi.help/2017/Coast_and_Sea/CycloneTool_Scientific_Doc.pdf, Last access: January 2020. 2017b.

Dullaart, J.C., Muis, S., Bloemendaal, N., Chertova, M.V., Couasnon, A. and Aerts, J.C., Accounting for TROPICAL CYCLONEs more than doubles the global population exposed to low-probability coastal flooding, Communications Earth & Environment, 2(1), pp.1-11, 2021.

Edmonds, D.A., Caldwell, R.L., Brondizio, E.S. and Siani, S.M., Coastal flooding will disproportionately impact people on river deltas, Nature communications, 11(1), pp.1-8, 2020

Emanuel, K.A. Downscaling CMIP5 climate models shows increased tropical cyclone activity over the 21st century, Proceedings of the National Academy of Sciences, 110(30), pp.12219-12224, 2013.

Emanuel, K., Response of global tropical cyclone activity to increasing CO2: Results from downscaling CMIP6 models, Journal of Climate, 34(1), pp.57-70, 2021.

Erban, L.E., Gorelick, S.M. and Zebker, H.A., Groundwater extraction, land subsidence, and sea-level rise in the Mekong Delta, Vietnam, Environmental Research Letters, 9(8), p.084010, 2014.

Feng, X., Klingaman, N.P. and Hodges, K.I., 2021. Poleward migration of western North Pacific tropical cyclones related to changes in cyclone seasonality. Nature communications, 12(1), pp.1-11.

Fox-Kemper, B., H. T. Hewitt, C. Xiao, G. Aðalgeirsdóttir, S. S. Drijfhout, T. L. Edwards, N. R. Golledge, M. Hemer, R. E. Kopp, G. Krinner, A. Mix, D. Notz, S. Nowicki, I. S. Nurhati, L. Ruiz, J-B. Sallée, A. B. A. Slangen, Y. Yu, Ocean, Cryosphere and Sea Level Change. In: Climate Change 2021: The Physical Science Basis. Contribution of Working Group I to the Sixth Assessment Report of the Intergovernmental Panel on Climate Change [Masson-Delmotte, V., P. Zhai, A. Pirani, S. L. Connors, C. Péan, S. Berger, N. Caud, Y. Chen, L. Goldfarb, M. I. Gomis, M. Huang, K. Leitzell, E. Lonnoy, J. B. R. Matthews, T. K. Maycock, T. Waterfield, O. Yelekçi, R. Yu and B. Zhou (eds.)]. Cambridge University Press, In Press, 2021.

Fritz, H.M., Blount, C.D., Thwin, S., Thu, M.K. and Chan, N., Cyclone Nargis storm surge in Myanmar, Nature Geoscience, 2(7), pp.448-449, 2009.

Gray, W.M., 1975. Tropical cyclone genesis (Doctoral dissertation, Colorado State University. Libraries).

Gray, W.M., Tropical Cyclone Genesis in the Western North Pacific. Journal of the Meteorological Society of Japan, 55(5).

Guo, S.L., A discussion on unbiased plotting positions for the general extreme value distribution, Journal of Hydrology, 121(1-4), pp.33-44, 1990.

GFDRR, Country Profile: Vietnam. https://www.gfdrr.org/en/publication/country-profile-vietnam, Last access: 12 December 2020, 2015.

Haigh, I.D., Eliot, M. and Pattiaratchi, C., Global influences of the 18.61 year nodal cycle and 8.85 year cycle of lunar perigee on high tidal levels, Journal of Geophysical Research: Oceans, 116(C6), 2011.

Haigh, I.D., MacPherson, L.R., Mason, M.S., Wijeratne, E.M.S., Pattiaratchi, C.B., Crompton, R.P. and George, S., Estimating present day extreme sea level exceedance probabilities around the coastline of Australia: tropical cyclone-induced storm surges, Climate Dynamics, 42(1-2), pp.139-157, 2014.

Haigh, I.D., Pickering, M.D., Green, J.M., Arbic, B.K., Arns, A., Dangendorf, S., Hill, D.F., Horsburgh, K., Howard, T., Idier, D. and Jay, D.A., 2020. The tides they are a-Changin': A comprehensive review of past and future nonastronomical changes in tides, their driving mechanisms, and future implications. Reviews of Geophysics, 58(1), p.e2018RG000636.

Harper, B.A. and Holland, G.J., An updated parametric model of the tropical cyclone, In Proc. 23rd Conf. Hurricanes and Tropical Meteorology, January 1999. (pp. 10-15). 1999.

Hausfather, Z. and Peters, G.P., Emissions-the 'business as usual' story is misleading, Nature, 577(7792), pp.618-621, 2020.

Hersbach, H., Bell, B., Berrisford, P., Biavati, G., Horányi, A., Muñoz Sabater, J., Nicolas, J., Peubey, C., Radu, R., Rozum, I., Schepers, D., Simmons, A., Soci, C., Dee, D., Thépaut, J-N., ERA5 hourly data on single levels from 1979 to present. Copernicus Climate Change Service (C3S) Climate Data Store (CDS). 10.24381/cds.adbb2d47, 2018.

Hinkel, J., Feyen, L., Hemer, M., Le Cozannet, G., Lincke, D., Marcos, M., Mentaschi, L., Merkens, J.L., de Moel, H., Muis, S. and Nicholls, R.J., 2021. Uncertainty and bias in global to regional scale assessments of current and future coastal flood risk. Earth's Future, 9(7), p.e2020EF001882.

Hinkel, J., Lincke, D., Vafeidis, A.T., Perrette, M., Nicholls, R.J., Tol, R.S., Marzeion, B., Fettweis, X., Ionescu, C. and Levermann, A., Coastal flood damage and adaptation costs under 21st century sea-level rise, Proceedings of the National Academy of Sciences, 111(9), pp.3292-3297, 2014.

Holland, G.J., An analytic model of the wind and pressure profiles in hurricanes, Monthly weather review, 108(8), pp.1212-1218, 1980.

Horsburgh, K. J. & Wilson, C., Tide-surge interaction and its role in the distribution of surge residuals in the North Sea. J. Geophys, Res. 112, C08003, 2007.

Hung, N.N., Delgado, J.M., Tri, V.K., Hung, L.M., Merz, B., Bárdossy, A. and Apel, H., Floodplain hydrology of the Mekong delta, Vietnam, Hydrological Processes, 26(5), pp.674-686, 2012.

Idier, D., Bertin, X., Thompson, P. and Pickering, M.D., Interactions between mean sea level, tide, surge, waves and flooding: mechanisms and contributions to sea level variations at the coast, Surveys in Geophysics, 40(6), pp.1603-1630, 2019.

Irish, J.L., Resio, D.T. and Divoky, D., Statistical properties of hurricane surge along a coast, Journal of Geophysical Research: Oceans, 116(C10), 2011.

IPCC. Climate Change and Land: an IPCC special report on climate change, desertification, land degradation, sustainable land management, food security, and greenhouse gas fluxes in terrestrial ecosystems [P.R. Shukla, J. Skea, E. Calvo Buendia, V. Masson-Delmotte, H.-O. Pörtner, D. C. Roberts, P. Zhai, R. Slade, S. Connors, R. van Diemen, M. Ferrat, E. Haughey, S. Luz, S. Neogi, M. Pathak, J. Petzold, J. Portugal Pereira, P. Vyas, E. Huntley, K. Kissick, M.Belkacemi, J. Malley, (eds.)], In press, 2019.

Jelesnianski, C.P., SPLASH : (Special Program to List Amplitudes of Surges from Hurricanes), I, Landfall storms, United States, National Weather Service., Techniques Development Laboratory, NOAA technical memorandum NWS TDL; 46, https://repository.library.noaa.gov/view/noaa/13509, 1972.

Kirezci, E., Young, I.R., Ranasinghe, R., Muis, S., Nicholls, R.J., Lincke, D. and Hinkel, J., Projections of global-scale extreme sea levels and resulting episodic coastal flooding over the 21st Century, Scientific reports, 10(1), pp.1-12, 2020.

Kleinen, J., Historical perspectives on typhoons and tropical storms in the natural and socio-economic system of Nam Dinh (Vietnam), Journal of Asian Earth Sciences, 29(4), pp.523-531, 2007.

Knabb, R.D., Rhome, R.R and Brown, D.P. Tropical Cyclone Report hurricane Katrina, 23 -30 August 2005. National Hurricane Center, https://www.nhc.noaa.gov/data/tcr/AL122005_Katrina.pdf. Last access: 15 December 2021, 2011.

Knapp, K. R., M. C. Kruk, D. H. Levinson, H. J. Diamond, and C. J. Neumann, The International Best Track Archive for Climate Stewardship (IBTrACS): Unifying tropical cyclone best track data. Bulletin of the American Meteorological Society, 91, 363-376, non-government domain doi:10.1175/2009BAMS2755.1, 2010.

Knutson, T., Camargo, S.J., Chan, J.C., Emanuel, K., Ho, C.H., Kossin, J., Mohapatra, M., Satoh, M., Sugi, M., Walsh, K. and Wu, L., Tropical cyclones and climate change assessment: Part II: Projected response to anthropogenic warming, Bulletin of the American Meteorological Society, 101(3), pp.E303-E322,

Kossin, J.P., Emanuel, K.A. and Vecchi, G.A., The poleward migration of the location of tropical cyclone maximum intensity, Nature, 509(7500), pp.349-352, 2014.

Lagmay, Alfredo Mahar Francisco, Rojelee P. Agaton, Mark Allen C. Bahala, Jo Brianne Louise T. Briones, Krichi May C. Cabacaba, Carl Vincent C. Caro, Lea L. Dasallas et al. , Devastating storm surges of Typhoon Haiyan, International journal of disaster risk reduction 11, pp1-12, 2015.

Lap, T.Q., Researching the variation of typhoon Intensities under climate change in Vietnam: A case study of typhoon Lekima, 2007, Hydrology, 6(2), p.51, 2019.

Larson, M., Hung, N.M., Hanson, H., Sundström, A. and Södervall, E., Impacts of Typhoons on the Vietnamese Coastline: A Case Study of Hai Hau Beach and Ly Hoa Beach, In Coastal Disasters and Climate Change in Vietnam (pp. 17-42), Elsevier, 2014.

Lin-Ye, J., García-León, M., Gràcia, V., Ortego, M.I., Lionello, P., Conte, D., Pérez-Gómez, B. and Sánchez-Arcilla, A., 2020. Modeling of future extreme storm surges at the NW Mediterranean Coast (Spain). Water,

12(2), p.472.Marcos, M., Calafat, F.M., Berihuete, Á. and Dangendorf, S., Long-term variations in global sea level extremes, Journal of Geophysical Research: Oceans, 120, 8115–8134, doi: 10.1002/2015JC011173, 2015.

Martin, P.J., Smith, S.R., Posey, P.G., Dawson, G.M. and Riedlinger, S.H., Use of the Oregon State University tidal inversion software (OTIS) to generate improved tidal prediction in the East-Asian Seas, Naval Research Lab Stennis Space Center MS Oceanography Div., 2009.

Mawdsley R.J. and Haigh I.D., Spatial and temporal variability and long-term trends in skew surges globally, Frontiers in Marine Science, 3:29, https://doi.org/10.3389/fmars.2016.00029, 2016.

McGranahan, G., Balk, D. and Anderson, B., The rising tide: assessing the risks of climate change and human settlements in low elevation coastal zones, Environment and urbanization, 19(1), pp.17-37, 2007.

Minderhoud, P.S.J., Erkens, G., Pham, V.H., Bui, V.T., Erban, L., Kooi, H. and Stouthamer, E., Impacts of 25 years of groundwater extraction on subsidence in the Mekong delta, Vietnam, Environmental research letters, 12(6), p.064006, 2017.

Mori, N., Shimura, T., Yoshida, K., Mizuta, R., Okada, Y., Fujita, M., Khujanazarov, T. and Nakakita, E., 2019. Future changes in extreme storm surges based on mega-ensemble projection using 60-km resolution atmospheric global circulation model. Coastal Engineering Journal, 61(3), pp.295-307.

Mousavi, M.E., Irish, J.L., Frey, A.E., Olivera, F. and Edge, B.L., Global warming and hurricanes: the potential impact of hurricane intensification and sea level rise on coastal flooding, Climatic Change, 104(3), pp.575-597, 2011.

Muis, S., Verlaan, M., Winsemius, H.C., Aerts, J.C. and Ward, P.J., A global reanalysis of storm surges and extreme sea levels, Nature communications, 7(1), pp.1-12, 2016.

Muis, S., Apecechea, M.I., Dullaart, J., de Lima Rego, J., Madsen, K.S., Su, J., Yan, K. and Verlaan, M., A High-resolution global dataset of extreme sea levels, tides, and storm surges, including future projections, Frontiers in Marine Science, 7, p.263, 2020.

Murakami, H. and Sugi, M., Effect of model resolution on tropical cyclone climate projections, Sola, 6, pp.73-76, 2010.

Nicholls, R.J., Storm surges in coastal areas. In: Arnold, M., Chen, R.S., Deichmann, U., Dilley, M., Lerner-Lam, A.L., Pullen, R.E. and Trohanis, Z. (eds.) Natural Disaster Hotspots Case Studies, The World Bank Hazard Management Unit, Disaster Risk Management Series, 6, pp.79-108, Washington, DC: World Bank, 2006.

Nicholls, R.J. and Cazenave, A., Sea-level rise and its impact on coastal zones. science, 328(5985), pp.1517-1520, 2010.

Nicholls, R.J., Lincke, D., Hinkel, J., Brown, S., Vafeidis, A.T., Meyssignac, B., Hanson, S.E., Merkens, J.L. and Fang, J., A global analysis of subsidence, relative sea-level change and coastal flood exposure, Nature Climate Change, pp.1-5, 2021.

Nguyen, H.N., Vu, K.T. and Nguyen, X.N., Flooding in Mekong River Delta, Viet Nam (No. HDOCPA-2007-53), Human Development Report Office (HDRO), United Nations Development Programme (UNDP), 2007.

Oppenheimer, M., B.C. Glavovic , J. Hinkel, R. van de Wal, A.K. Magnan, A. Abd-Elgawad, R. Cai, M. Cifuentes-Jara, R.M. DeConto, T. Ghosh, J. Hay, F. Isla, B. Marzeion, B. Meyssignac, and Z. Sebesvari, Sea Level Rise and Implications for Low-Lying Islands, Coasts and Communities. In: IPCC Special Report on the Ocean and Cryosphere in a Changing Climate [H.-O. Pörtner, D.C. Roberts, V. Masson-Delmotte, P. Zhai, M. Tignor, E. Poloczanska, K. Mintenbeck, A. Alegría, M. Nicolai, A. Okem, J. Petzold, B. Rama, N.M. Weyer (eds.)], 2019.

Pandey, S. and Rao, A.D., Impact of approach angle of an impinging cyclone on generation of storm surges and its interaction with tides and wind waves, Journal of Geophysical Research: Oceans, 124(11), pp.7643-7660, 2019.

Pasch, R.J., Penny, A.B. and Berg, R., Tropical Cyclone Report: Hurricane Maria. National Hurricane center, TC REPORT AL152017, National Oceanic And Atmospheric Administration and the National Weather Service, pp.1-48, 2018.

Pawlowicz, R., B. Beardsley, and S. Lentz, Classical Tidal Harmonic Analysis Including Error Estimates in MATLAB using T_TIDE, Computers and Geosciences, 28, 929-937, 2002

Peng, D., Hill, E.M., Meltzner, A.J. and Switzer, A.D., Tide gauge records show that the 18.61-year nodal tidal cycle can change high water levels by up to 30 cm, Journal of Geophysical Research: Oceans, 124(1), pp.736-749, 2019.

Phan, H.M., Ye, Q., Reniers, A.J. and Stive, M.J., Tidal wave propagation along The Mekong deltaic coast, Estuarine, Coastal and Shelf Science, 220, pp.73-98, 2019.

Poulose, J., Rao, A.D. and Bhaskaran, P.K., Role of continental shelf on non-linear interaction of storm surges, tides and wind waves: An idealized study representing the west coast of India, Estuarine, Coastal and Shelf Science, 207, pp.457-470, 2018.

Pugh, D. and Woodworth, P., Sea-level science: understanding tides, surges, tsunamis and mean sea-level changes, Cambridge University Press, 2014.

Ramos-Valle, A.N., Curchitser, E.N. and Bruyère, C.L., Impact of tropical cyclone landfall angle on storm surge along the Mid-Atlantic bight, Journal of Geophysical Research: Atmospheres, 125(4), p.e2019JD031796, 2020.

Rego, J.L. and Li, C., Nonlinear terms in storm surge predictions: Effect of tide and shelf geometry with case study from Hurricane Rita, Journal of Geophysical Research: Oceans, 115(C6), 2010.

Simpson, R.H. and Saffir, H., The hurricane disaster potential scale, Weatherwise, 27(8), p.169, 1974.

Santos-Burgoa, C., Goldman, A., Andrade, E., Barrett, N., Colon-Ramos, U., Edberg, M., Garcia-Meza, A., Goldman, L., Roess, A., Sandberg, J. and Zeger, S., Ascertainment of the estimated excess mortality from hurricane Maria in Puerto Rico, Himmelfarb Health Sciences Library, The George Washington University, Health Sciences Research Commons, Global Health Faculty Publications, Retrieved from https://hsrc.himmelfarb.gwu.edu/sphhs_global_facpubs/288, 2018.

Saulter, A., Bunney, C., Li, J.G. and Palmer, T., 2017, September. Process and resolution impacts on UK coastal wave predictions from operational global-regional wave models. In Proceedings of the 15th International Workshop on Wave Hindcasting and Forecasting and 6th Coastal Hazard Symposium, Liverpool, UK (pp. 10-15).

Seneviratne, S.I., Nicholls, N., Easterling, D., Goodess, C., Kanae, S., Kossin, J., Luo, Y., Marengo, J., McInnes, K., Rahimi, M. and Reichstein, M., Managing the risks of extreme events and disasters to advance climate change adaptation, A special report of working Groups I and II of the Intergovernmental Panel on Climate Change (IPCC), 2012.

SwissRe, Industry-first Global Storm Surge Zones, https://www.swissre.com/dam/jcr:dedf399f-af17-4061-928f-dba8229c1499/industry_first_global_storm_surge_zones.pdf, Last access: 25 January 2021, 2017.

Tadesse, M.G. and Wahl, T., A database of global storm surge reconstructions, Scientific Data, 8(1), pp.1-10, 2021.

Takagi, H., Thao, N.D., Esteban, M., Tran, T.T., Knaepen, H.L., Mikami, T. Vulnerability of coastal areas in southern Vietnam against tropical cyclones and storm surges, In Proceedings of the 4th International Conference on Estuaries and Coasts (ICEC), Hanoi, Vietnam, 8–11 October 2012, pp. 292–299. 2012.

Takagi, H., Esteban, M., Shibayama, T., Mikami, T., Matsumaru, R., De Leon, M., Thao, N.D., Oyama, T. and Nakamura, R., Track analysis, simulation, and field survey of the 2013 Typhoon Haiyan storm surge, Journal of Flood Risk Management, 10(1), pp.42-52, 2017.

Tozer, B., Sandwell, D.T., Smith, W.H.F., Olson, C., Beale, J.R. and Wessel, P., Global bathymetry and topography at 15 arc sec: SRTM15+. Earth and Space Science, 6(10), pp.1847-1864, 2019.

OCHA (UN Office for the Coordination of Humanitarian Affairs), Typhoon Bopha Situation Report No. 19. https://reliefweb.int/report/philippines/typhoon-bopha-situation-report-no-19-12-february-2013. Last access: 25 January 2021, 2013.

Vitousek, S., Barnard, P.L., Fletcher, C.H., Frazer, N., Erikson, L. and Storlazzi, C.D., 2017. Doubling of coastal flooding frequency within decades due to sea-level rise. Scientific reports, 7(1), pp.1-9.

Voldoire, A., Sanchez-Gomez, E., y Mélia, D.S., Decharme, B., Cassou, C., Sénési, S., Valcke, S., Beau, I., Alias, A., Chevallier, M. and Déqué, M., The CNRM-CM5. 1 global climate model: description and basic evaluation, Climate dynamics, 40(9), pp.2091-2121, 2013.

Vousdoukas, M.I., Voukouvalas, E., Annunziato, A., Giardino, A. and Feyen, L., Projections of extreme storm surge levels along Europe, Climate Dynamics, 47(9), pp.3171-3190, 2016.

Wahl, T. and Chambers, D.P., Climate controls multidecadal variability in US extreme sea level records, Journal of Geophysical Research: Oceans, 121(2), pp.1274-1290, 2016.

Wahl, T., Haigh, I.D., Nicholls, R.J., Arns, A., Dangendorf, S., Hinkel, J. and Slangen, A.B., Understanding extreme sea levels for broad-scale coastal impact and adaptation analysis, Nature communications, 8(1), pp.1-12, 2017.

Williams, J., Horsburgh, K.J., Williams, J. A. & Proctor, R.N.F., Tide and skew surge independence: new insights for flood risk, Geophys. Res. Lett., https://doi.org/10.1002/2016GL069522, 2016.

WMO (World Meteorological Organization), Storm Surge, https://public.wmo.int/en/our-mandate/focus-areas/natural-hazards-and-disaster-risk-reduction/storm-surge, Last access: 21 January 2021, 2021.

Woodruff, J.D., Irish, J.L. and Camargo, S.J., Coastal flooding by tropical cyclones and sea-level rise, Nature, 504(7478), pp.44-52, 2013.

Wong, P.P., I.J. Losada, J.-P. Gattuso, J. Hinkel, A. Khattabi, K.L. McInnes, Y. Saito, and A. Sallenger, Coastal systems and low-lying areas. In: Climate Change 2014: Impacts, Adaptation, and Vulnerability. Part A:Global and Sectoral Aspects. Contribution of Working Group II to the Fifth Assessment Report of the Intergovernmental Panel on Climate Change [Field, C.B., V.R. Barros, D.J. Dokken, K.J. Mach,M.D. Mastrandrea, T.E. Bilir, M. Chatterjee, K.L. Ebi, Y.O. Estrada, R.C. Genova, B. Girma, E.S. Kissel, A.N. Levy,S. MacCracken, P.R. Mastrandrea, and L.L. White (eds.)], Cambridge University Press, Cambridge, United Kingdom and New York, NY, USA, pp. 361-409, 2014.

Zhang, B. and Wang, S., Probabilistic characterization of extreme storm surges induced by tropical cyclones, Journal of Geophysical Research: Atmospheres, 126(3), p.e2020JD033557, 2021.